Physics in Medicine & Biology

PAPER

Analytical probabilistic modeling of RBE-weighted dose for ion therapy

IOP Publishing | Institute of Physics and Engineering in Medicine Physics in Medicine & Biology

Phys. Med. Biol. **62** (2017) 8959–8982 https://doi.org/10.1088/1361-6560/aa915d

Analytical probabilistic modeling of RBE-weighted dose for ion therapy

H P Wieser[1,2], P Hennig[3], N Wahl[1,2] and M Bangert[1,2]

[1] Department of Medical Physics in Radiation Oncology, German Cancer Research Center—DKFZ, Im NeuenheimerFeld 280, D-69120 Heidelberg, Germany
[2] Heidelberg Institute for Radiation Oncology—HIRO, Im Neuenheimer Feld 280, D-69120, Germany
[3] Max Planck Institute for Intelligent Systems, Spemannstraße 34, 72076 Tübingen, Germany

E-mail: h.wieser@dkfz.de

Received 28 May 2017, revised 27 September 2017
Accepted for publication 5 October 2017
Published 10 November 2017

Abstract

Particle therapy is especially prone to uncertainties. This issue is usually addressed with uncertainty quantification and minimization techniques based on scenario sampling. For proton therapy, however, it was recently shown that it is also possible to use closed-form computations based on analytical probabilistic modeling (APM) for this purpose. APM yields unique features compared to sampling-based approaches, motivating further research in this context.

This paper demonstrates the application of APM for intensity-modulated carbon ion therapy to quantify the influence of setup and range uncertainties on the RBE-weighted dose. In particular, we derive analytical forms for the nonlinear computations of the expectation value and variance of the RBE-weighted dose by propagating linearly correlated Gaussian input uncertainties through a pencil beam dose calculation algorithm. Both exact and approximation formulas are presented for the expectation value and variance of the RBE-weighted dose and are subsequently studied in-depth for a one-dimensional carbon ion spread-out Bragg peak. With V and B being the number of voxels and pencil beams, respectively, the proposed approximations induce only a marginal loss of accuracy while lowering the computational complexity from order $\mathcal{O}(V \times B^2)$ to $\mathcal{O}(V \times B)$ for the expectation value and from $\mathcal{O}(V \times B^4)$ to $\mathcal{O}(V \times B^2)$ for the variance of the RBE-weighted dose. Moreover, we evaluated the approximated calculation of the expectation value and standard deviation of the RBE-weighted dose in combination with a probabilistic effect-based optimization on three patient cases considering carbon ions as radiation modality against sampled references. The resulting

global γ-pass rates (2 mm,2%) are >99.15% for the expectation value and > 94.95% for the standard deviation of the RBE-weighted dose, respectively. We applied the derived analytical model to carbon ion treatment planning, although the concept is in general applicable to other ion species considering a variable RBE.

Keywords: probabilistic treatment planning, biological effect, particle therapy, carbon ion, treatment planning

(Some figures may appear in colour only in the online journal)

1. Introduction

Treatment planning for charged particle therapy requires an accurate simulation of the dose distribution within the patient's body before delivery. In reality, various sources of uncertainty along the treatment planning work-flow, e.g. imaging, dose calculation, or irradiation itself, may impair the validity of the simulated dose distributions. Range and setup uncertainties are considered to be among the most influential sources of physical uncertainty (Lomax 2008a, 2008b, Paganetti 2012). Their dosimetric impact can be quantified using worst case estimates (Albertini *et al* 2011, Liu *et al* 2013, Lowe *et al* 2016), dose blurring methods (Baum *et al* 2004), dose warping techniques (Park *et al* 2012), sampling meta models based on Gaussian processes (Sobotta *et al* 2012), and polynomial chaos expansion (Perkó *et al* 2016).

The afore-mentioned uncertainties are compensated during treatment planning in current clinical practice by the design of an adequate margin, which extends the clinical target volume (CTV) to a planning target volume (van Herk 2004). This approach is either restricted to non-problematic cases where anatomical variations do not imply strong modifications of radiological depths or are combined with single field uniform dose (SFUD) optimization (Lomax 2008c). Robust optimization techniques such as worst case (Pflugfelder *et al* 2008, Fredriksson *et al* 2011, Chen *et al* 2012, Liu *et al* 2012) or probabilistic optimization (Unkelbach *et al* 2007, 2009) are designed to supersede safety margins. While initial commercial implementations are available for proton therapy, no commercial implementations are available for carbon ion therapy.

In contrast to protons, studies in robust treatment planning for heavier charged particles, such as carbon ions, are very limited. As carbon ion dose distributions exhibit steeper lateral and longitudinal dose gradients—in particular in the high dose domain directly around the target—robustness analysis and robust optimization may arguably be especially important for this modality (Suit *et al* 2010). Meaningful consideration requires nonlinear modeling of the relative biological effectiveness (RBE) of carbon ions yielding a more complex treatment planning process than for protons (Jäkel *et al* 2001). Steitz *et al* (2016) studied the dosimetric impact of interfactional motion on pancreatic cancer, applying worst case, SFUD and margin-based optimization, and concluding that robust optimization is a valuable tool to improve the trade-off between robust target coverage and organ at risk sparing. Sakama *et al* (2016) estimated the variance of the biological effective dose considering fractionation effects by using a fast dose wrapping technique based on the water equivalent path length.

At their core, all previously referenced methods rely on sampling, i.e. the simulation of a discrete set of treatment scenarios. Inevitably, this results in a trade-off between the accuracy

of uncertainty propagation and computational cost which is negatively affected by an increasing number of uncertain input parameters and complex correlations of the uncertainties, especially with regard to fractionation.

For intensity-modulated proton therapy, it is possible to bypass the need for sampling through the use of analytical probabilistic modeling (APM) that enables closed-form calculation of the expectation value and standard deviation of the RBE-weighted dose considering a constant RBE of 1.1 (Bangert *et al* 2013). APM facilitates the incorporation of arbitrary correlation models, including fractionation effects of range and setup errors, at an improved accuracy to efficiency trade-off compared to conventional sampling approaches (Wahl *et al* 2017). As a further consequence, highly efficient probabilistic optimization is possible.

In this paper, we generalize APM computations of the expectation value and the variance from the linear dose calculation required for proton therapy to nonlinear RBE-weighted dose calculation for carbon ions. An accurate mathematical model depicting the complex dependence of RBE on dose requires the joint incorporation of range and setup uncertainties into the physical dose and RBE at the same time. Because the underlying mathematical moment computations are computationally challenging, algebraic approximations that effectively reduce complexity are introduced. The quality of the approximations are investigated in detail for a one-dimensional (1D) spread-out Bragg peak (SOBP). In addition, we investigate APM's accuracy compared to sampling-based approaches on three patient cases and perform a treatment planning study using probabilistic biological effect optimization under different fractionation assumptions.

This paper is organized as follows. Section 2 repeats the basic principle of APM and derives calculations for the nominal value, expectation value, and variance of the biological effect ε and RBE-weighted dose. Next, section 3 shows the application on a 1D SOBP and three patient cases considering different fractionation schemes. Sections 4 and 5 discuss and conclude the paper.

2. Material and methods

At the same physical dose, carbon ions induce a lower cell survival rate than protons, mainly due to differences in the microscopic energy deposition pattern. Hence, clinical carbon ion treatment planning is based on the RBE-weighted dose with the RBE being a patient-specific nonlinear three-dimensional (3D) quantity depending, among other things, on linear energy transfer, dose level, biological endpoint, and tissue type. The RBE is defined as the ratio between iso-effective physical doses of a reference radiation d_x and of particles d_p. In the framework of the linear quadratic (LQ) model (Kellerer and Rossi 1978), the RBE-weighted dose is given by

$$\mathrm{RBE} \times d_p = \sqrt{\frac{\alpha_p d_p + \beta_p d_p^2}{\beta_x} + \left(\frac{\alpha_x}{2\beta_x}\right)^2} - \frac{\alpha_x}{2\beta_x} \tag{1}$$

with the parameters α_x, β_x (α_p, β_p) describing the radio-sensitivity of photons (particles). The computation of the RBE-weighted dose involves an intermediate quantity, i.e. the biological effect

$$\varepsilon_p = \alpha_p d_p + \beta_p d_p^2 \tag{2}$$

which can be used as an alternative for treatment planning (Wilkens and Oelfke 2006). Via the LQ model, ε_p is linked to cell survival S

$$S = \mathrm{e}^{-\varepsilon_p} = \mathrm{e}^{-\alpha_p d_p - \beta_p d_p^2}. \tag{3}$$

For algebraic convenience, we focus on the biological effect ε of building an analytical probabilistic model for uncertainty propagation and not on the RBE-weighted dose. An explanation for this approach will be given at a later point where it is shown that the square root dependence in equation (1) can be accounted for with a post processing step (see section 2.6) to ultimately obtain the desired mean and variance of the RBE-weighted-dose.

The biological effect $\boldsymbol{\varepsilon}(X)$ is considered to be a function of uncertain input parameters X that follow a probability density $p(X)$. Consequently, the n-th raw moment of the induced probability distribution over the biological effect ε can be calculated/approximated by

$$\mathbb{E}[\boldsymbol{\varepsilon}(X)^n] = \int \mathrm{d}X\, p(X)\boldsymbol{\varepsilon}(X)^n \approx \int \mathrm{d}X\, \mathcal{N}(X, \bar{X}, \Sigma_X)\, \hat{\boldsymbol{\varepsilon}}(X)^n. \tag{4}$$

Equation (4) shows the basic concept of APM. Using a multivariate normal distribution $\mathcal{N}(X, \bar{X}, \Sigma_X)$ to describe the probability distribution over uncertain input parameters $p(X)$ and using a functional approximation $\hat{\boldsymbol{\varepsilon}}$ instead of the full form $\boldsymbol{\varepsilon}$, we aim at solving the integral equation in closed form. The main challenge is therefore to identify a functional approximation $\hat{\boldsymbol{\varepsilon}}$ that allows for high approximation quality and minimal computational cost at the same time.

In the following, we are going to introduce, step-by-step, the functional approximation $\hat{\boldsymbol{\varepsilon}}$ (section 2.1), the uncertainty model (section 2.2), and the solution of equation (4) to compute the expectation value and variance of $\boldsymbol{\varepsilon}$ (sections 2.3 and 2.4). Finally, section 2.7 outlines the validation. In the following, i, l refer to voxel indices, j, m, o refer to pencil beam indices, V denotes the number of dose voxels and B depicts the number of pencil beams.

2.1. Nominal biological effect calculation

Throughout this work, we focus on carbon ions and obtain their tissue response ($\alpha(T,E)$, $\beta(T,E)$) from the tissue response to x-rays using the local effect model IV (LEM IV) (Scholz and Kraft 1996, Elsässer *et al* 2010). Given the particle fluence $\Phi(z,T,E)$, the stopping power $SP(T,E)$, the particle type T, the energy E and the radiological depth z, we follow Zaider and Rossi (1980) to obtain a depth-dependent dose-averaged LQ model parameter for each initial beam energy:

$$\alpha^c(z) = \frac{\sum_T \int_0^\infty \alpha(T,E)\, \Phi(z,T,E)\, SP(T,E)\, \mathrm{d}E}{\sum_T \int_0^\infty \Phi(z,T,E)\, SP(T,E)\, \mathrm{d}E}. \tag{5}$$

A similar expression can be derived for $\sqrt{\beta^c(z)}$, but is not shown here. We decided to use LEM as it is also used for clinical treatment planning in European carbon ion therapy centers. Photon reference radio-sensitivity parameters of $\alpha_x = 0.1\ \mathrm{Gy}^{-1}$ and $\beta_x = 0.05\ \mathrm{Gy}^{-2}$ were used as an LEM input, but our considerations are neither restricted to these tissue-specific values nor to LEM IV. To assess the biological effects for an ensemble of particles, we follow Krämer and Scholz (2006) which limits our considerations to doses $\leqslant$10 Gy(RBE).

For treatment planning, we use 121 tabulated carbon ion depth dose profiles, spaced from 115.23 MeV u^{-1}–398.84 MeV u^{-1}. Each integrated physical dose profile is scored as a function of depth in water and complemented by dose-averaged $\boldsymbol{\alpha}^c$—and $\boldsymbol{\beta}^c$ profiles considering the particle spectra.

Lateral dose profiles of the carbon pencil beam are parameterized as a function of depth by a single radially symmetric Gaussian. The total width of the carbon ion beam at radiological depth z is determined by the initial beam width and the beam broadening caused by multiple Coloumb scattering $\lambda^2 = \sigma^2_{\text{Ini}} + \sigma^2_{\text{MC}}(z)$. By this means, depth-dependent characteristics of each of the 121 pencil beams are described by four vectors ($d(z)$, $\alpha^c(z)$, $\sqrt{\beta^c}(z)$ and $\sigma^2_{\text{MC}}(z)$) and are part of the base data used for treatment planning.

The implemented dose calculation in water is based on the pencil beam algorithm presented in Schaffner *et al* (1999) and includes a full volumetric ray tracing (Siggel *et al* 2012). A detailed description of the underlying carbon dose calculation engine and comparison to a validated treatment planning system can be found elsewhere (Wieser *et al* 2017).

To account for the synergistic effects in a mixed radiation field created by ions of different energies, the calculation of the total biological effect ε_i at voxel i requires the calculation of dose-averaged radio-sensitivity parameters α^c_i and $\sqrt{\beta^c_i}$ taking into account contributions from different spots (Zaider and Rossi 1980). Let w_j be the fluence weight of pencil beam j and D_{ij} ($\alpha^c_{ij}/\sqrt{\beta^c_{ij}}$) the dose (LQ model parameter) contribution of pencil beam j to voxel i. The nominal biological effect ε_i is then given by Wilkens and Oelfke (2006):

$$\varepsilon_i(\boldsymbol{w}) = \alpha^c_i(\boldsymbol{w})d_i(\boldsymbol{w}) + \beta^c_i(\boldsymbol{w})d^2_i(\boldsymbol{w}) = \sum_{j=1}^{B} w_j \alpha^c_{ij} D_{ij} + \left(\sum_{j=1}^{B} w_j \sqrt{\beta}^c_{ij} D_{ij}\right)^2 . \tag{6}$$

To reduce the number of computations for the calculation of the biological effect in the context of APM, physical $d(z)$ and biological beam properties $\alpha^c(z)$, $\sqrt{\beta^c}(z)$ were combined for each initial energy by multiplying the integrated depth dose profile with each of the two dose-averaged radio-sensitivity parameters of the LQ model upfront. The $\circ$ operator represents in the following the element-wise multiplication (Hadamard product) of two vectors $\boldsymbol{u}$ and $\boldsymbol{v}$, i.e. for element x of the resulting vector we have $(u \circ v)_x = u_x \cdot v_x$. The resulting $\boldsymbol{\alpha^c} \circ \boldsymbol{d}$ and $\boldsymbol{\sqrt{\beta^c}} \circ \boldsymbol{d}$ profiles enable a direct derivation of the biological effect for each individual pencil beam. The elementwise multiplication can be understood as modeling a perfect correlation between the physical dose and its biological beam properties. A change in range, e.g. due to range uncertainties, consistently changes the corresponding depth-dependent dose-averaged $\alpha^c(z)$ and $\sqrt{\beta^c}(z)$ profiles and further the RBE-weighted dose. This assumption is inspired by equation (6) and requires then only three ($\boldsymbol{\alpha^c} \circ \boldsymbol{d}$, $\boldsymbol{\sqrt{\beta^c}} \circ \boldsymbol{d}$ and $\boldsymbol{\sigma^2_{\text{MC}}}$) instead of four depth-dependent components to describe the characteristics of a carbon ion pencil beam.

In agreement with the conventional pencil beam model, we assume a factorization into two lateral dose components L^x_{ij}, L^y_{ij} and one depth dose component, Z^{α}_{ij} and $Z^{\sqrt{\beta}}_{ij}$, respectively. Thus, the biological effect can be reformulated as

$$\varepsilon_i = \sum_{j=1}^{B} w_j L^x_{ij} L^y_{ij} Z^{\alpha}_{ij} + \left(\sum_{j=1}^{B} w_j L^x_{ij} L^y_{ij} Z^{\sqrt{\beta}}_{ij}\right)^2 . \tag{7}$$

Similar to Wilkens and Oelfke (2006) we are assuming laterally constant α^c and β^c, which implies they only influence the depth-dependent components in equations (6) and (7). In analogy to the physical depth dose for protons (Bangert *et al* 2013), we represent depth-dependent $\boldsymbol{\alpha^c} \circ \boldsymbol{d}$ and $\boldsymbol{\sqrt{\beta^c}} \circ \boldsymbol{d}$ profiles by a weighted superposition of 13 Gaussian components. Compared to Bangert *et al* (2013) we increased the number of Gaussian components by three due to the sharper peak and the additional fragmentation tail that needs to be modeled. Herewith, we switch to a representation of the tabulated base data that now allows analytical

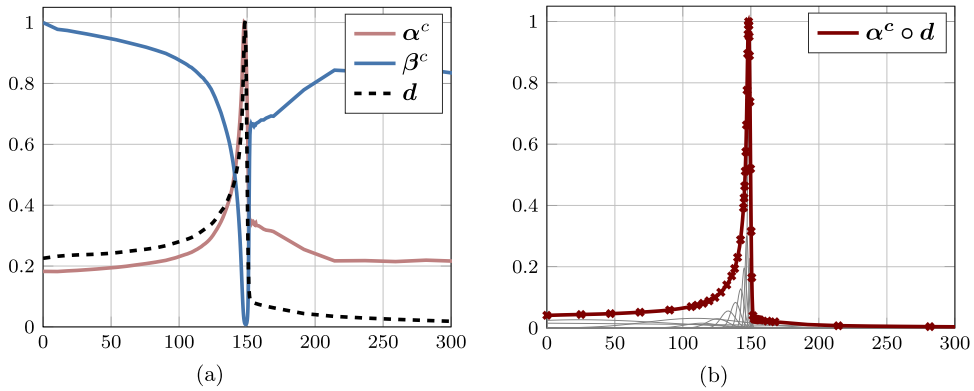

Figure 1. (a) Normalized integrated carbon ion depth dose profile of a 227 MeV u^{-1} beam (dashed black line) and corresponding dose-averaged $\boldsymbol{\alpha}^c$ (solid red) and $\boldsymbol{\beta}^c$ (solid blue) curves of the LQ model predicted by LEM IV using $\alpha_x = 0.1\,\mathrm{Gy}^{-1}$ and $\beta_x = 0.05$ Gy^{-2}. (b) $\boldsymbol{\alpha}^c \circ \boldsymbol{d}$—profile (red solid line) of a 277 MeV carbon ion beam represented by a weighted superposition of 13 Gaussian components (solid grey). Crosses indicate reference values. (a) z (mm). (b) z (mm).

integration. Least-squares fits for 121 initial beam energies were carried out as an off-line pre-computation (i.e. they yield tabulated coefficients that do not have to be reproduced at runtime). Thus, each pair of curves is described according to equation (8) with a set of weights ω_{jk}^{α} ω_{jk}^{β}, means μ_{jk}^{α}, μ_{jk}^{β} and widths δ_{jk}^{α}, δ_{jk}^{β}. It is noteworthy that each set of photon reference radio-sensitivity parameters requires a new fit.

Given the radiological depth z_{ij} of voxel i irradiated by pencil beam j, Z_{ij}^{α} and $Z_{ij}^{\sqrt{\beta}}$ can be obtained via:

$$Z_{ij}^{\alpha} = \sum_{k=1}^{13} \frac{\omega_{jk}^{\alpha}}{\sqrt{2\pi\delta_{jk}^{\alpha\,2}}} \mathrm{e}^{\frac{\left(z_{ij}-\mu_{jk}^{\alpha}\right)^2}{2\delta_{jk}^{\alpha\,2}}} \quad \text{and} \quad Z_{ij}^{\sqrt{\beta}} = \sum_{k=1}^{13} \frac{\omega_{jk}^{\beta}}{\sqrt{2\pi\delta_{jk}^{\beta\,2}}} \mathrm{e}^{\frac{\left(z_{ij}-\mu_{jk}^{\beta}\right)^2}{2\delta_{jk}^{\beta\,2}}}. \tag{8}$$

Figure 1(a) depicts the physical and biological beam properties of a single energy carbon ion beam of 277 MeV u^{-1} and figure 1(b) illustrates the achieved fit for the corresponding $\boldsymbol{\alpha}^c \circ \boldsymbol{d}$ profile. The mean relative difference in the reference data amounts to 0.25% for $\boldsymbol{\alpha}^c \circ \boldsymbol{d}$ profiles and 0.06% for $\sqrt{\boldsymbol{\beta}^c} \circ \boldsymbol{d}$ profiles.

Next, let x_{ij}/y_{ij} be the lateral distances of voxel i to the central ray of pencil beam j, λ_{ij}^2 be the beam width of voxel i and pencil beam j at radiological depth z_{ij}, $\mathcal{N}(x;\mu,\lambda)$ be a Gaussian distribution with mean μ and standard deviation λ evaluated at x, then equation (7) can be rewritten to only rely on Gaussian components:

$$\begin{aligned}\varepsilon_i = &\sum_{j=1}^{B} w_j \mathcal{N}(x_{ij};\mu_j^x,\lambda_{ij})\,\mathcal{N}(y_{ij};\mu_j^y,\lambda_{ij}) \sum_{k=1}^{13} \omega_{jk}^{\alpha}\,\mathcal{N}(z_{ij};\mu_{jk}^{\alpha},\delta_{jk}^{\alpha}) \\ &+ \left(\sum_{j=1}^{B} w_j \mathcal{N}(x_{ij};\mu_j^x,\lambda_{ij})\,\mathcal{N}(y_{ij};\mu_j^y,\lambda_{ij}) \sum_{k=1}^{13} \omega_{jk}^{\beta}\,\mathcal{N}(z_{ij};\mu_{jk}^{\beta},\delta_{jk}^{\beta})\right)^2. \end{aligned} \tag{9}$$

Consequently, equation (9) renders the calculation of the expectation value and variance of the biological effect according to equation (4) analytically tractable.

2.2. Uncertainty model

Setup and range errors are considered individually for each pencil beam by modeling offsets $\boldsymbol{\Delta}^x \in \mathbb{R}^B$, $\boldsymbol{\Delta}^y \in \mathbb{R}^B$, and $\boldsymbol{\Delta}^z \in \mathbb{R}^B$ in the Gaussian components underlying the biological effect calculation

$$\varepsilon_i = \sum_{j=1}^{B} w_j \mathcal{N}(x_{ij} + \Delta_j^x; \mu_j^x, \lambda_{ij}) \mathcal{N}(y_{ij} + \Delta_j^y; \mu_j^y, \lambda_{ij}) \sum_{k=1}^{13} \omega_{jk}^{\alpha} \mathcal{N}(z_{ij} + \Delta_j^z; \mu_{jk}^{\alpha}, \delta_{jk}^{\alpha}) + \left(\sum_{j=1}^{B} w_j \mathcal{N}(x_{ij} + \Delta_j^x; \mu_j^x, \lambda_{ij}) \mathcal{N}(y_{ij} + \Delta_j^y; \mu_j^y, \lambda_{ij}) \sum_{k=1}^{13} \omega_{jk}^{\beta} \mathcal{N}(z_{ij} + \Delta_j^z; \mu_{jk}^{\beta}, \delta_{jk}^{\beta}) \right)^2 . \tag{10}$$

$\boldsymbol{\Delta}^x$, $\boldsymbol{\Delta}^y$, and $\boldsymbol{\Delta}^z$ stem from a joint probability distribution $p(\boldsymbol{\Delta}^x, \boldsymbol{\Delta}^y, \boldsymbol{\Delta}^z)$ which factorizes into a product of three multivariate normal distributions with zero mean

$$p(\boldsymbol{\Delta}^x, \boldsymbol{\Delta}^y, \boldsymbol{\Delta}^z) = \mathcal{N}(\boldsymbol{\Delta}^x; 0, \Sigma^x) \mathcal{N}(\boldsymbol{\Delta}^y; 0, \Sigma^y) \mathcal{N}(\boldsymbol{\Delta}^z; 0, \Sigma^z). \tag{11}$$

The covariance matrices Σ^x, Σ^y, Σ^z allow us to explicitly model the magnitude of uncertainty of arbitrary pairwise pencil beam correlations and have to be defined upfront according to the uncertainty assumptions. Here, we assume setup errors to be perfectly correlated for pencil beams belonging to the same beam direction, whereas pencil beam pairs stemming from different beam directions are uncorrelated. Range uncertainties are perfectly correlated for pencil beams impinging on the same lateral position as carbon ions and fragments penetrate the same tissue (Unkelbach *et al* 2009).

The APM formalism allows us to consider fractionation effects by exploiting a correlation model on the interplay of systematic and random errors over multiple treatment fractions. Thereby, the computation complexity is constant for an increasing number of fractions (Bangert *et al* 2013). Throughout this article, setup errors are assumed to be comprised of a 1 mm systematic- and a 2 mm random-error. In addition, range errors are described by a relative systematic error component of 3.5% and a random error of 1 mm.

The probability density $p(\boldsymbol{\Delta}^x, \boldsymbol{\Delta}^y, \boldsymbol{\Delta}^z)$ induces uncertainty over ε_i that can be described with a probability distribution $p(\varepsilon_i)$ which is of non-Gaussian form. The functional approximation of the biological effect calculation along with the uncertainty assumptions made in this section enable the calculation of statistical moments of the biological effect $\boldsymbol{\varepsilon}$ in closed-form. Hence, analytical expressions for the expectation value $\mathbb{E}[\boldsymbol{\varepsilon}]$ and the covariance matrix $\mathbb{E}[\boldsymbol{\varepsilon}\boldsymbol{\varepsilon}^T] - \mathbb{E}[\boldsymbol{\varepsilon}]\mathbb{E}[\boldsymbol{\varepsilon}]^T$ can be derived. Here $\mathbb{E}[\cdot]$ denotes the expectation operator. In general, it is also possible to obtain an analytical expression for higher order moments (e.g. skewness, kurtosis) to better describe the unknown shape of the probability density of $p(\varepsilon_i)$, but this is beyond the scope of this paper.

2.3. Expected biological effect

To increase the readability for the following deviations, appendix A depicts a lookup table A1 explaining the notation employed in this section. To calculate the expectation value, i.e. the first raw moment of the biological effect in closed-form considering setup and range uncertainties, equation (12) needs to be solved:

$$\mathbb{E}[\varepsilon_i] = \int \mathrm{d}\boldsymbol{\Delta}^x \mathrm{d}\boldsymbol{\Delta}^y \mathrm{d}\boldsymbol{\Delta}^z \, p(\boldsymbol{\Delta}^x) \, p(\boldsymbol{\Delta}^y) \, p(\boldsymbol{\Delta}^z) \varepsilon_i(\boldsymbol{\Delta}^x, \boldsymbol{\Delta}^y, \boldsymbol{\Delta}^z). \tag{12}$$

The computations require standard Gaussian algebra as exercised in appendix B or in equations (13)–(18) in Bangert *et al* (2013) yielding the form

$$\mathbb{E}[\varepsilon_i] = \sum_{j}^{B} w_j \mathcal{L}_{ij}^{x} \mathcal{L}_{ij}^{y} \mathcal{Z}_{ij}^{\alpha} + \sum_{jm}^{B} w_j w_m \Upsilon_{ijim}^{x} \Upsilon_{ijim}^{y} \Xi_{ijim}^{\sqrt{\beta}}. \tag{13}$$

Due to the quadratic term in the biological effect, the calculation of its expectation value requires the 4th order terms $\Upsilon_{ijim}^{x/y}$ and $\Xi_{ijim}^{\sqrt{\beta}}$, representing the second raw moment of $L_{ij}^{x/y}$, $Z_{ij}^{\sqrt{\beta}}$. These 4th order terms model the influence of pencil beam combinations jm of the quadratic term on the expected biological effect $\mathbb{E}[\varepsilon_i]$ and emerge by integrating the biological effect ε_i against Gaussian densities, as illustrated in equation (12). However, for fraction doses of individual pencil beams, we have $\boldsymbol{\alpha}^{\boldsymbol{c}} \circ \boldsymbol{d} \gg (\sqrt{\boldsymbol{\beta}^{\boldsymbol{c}}} \circ \boldsymbol{d})^2$ and consequently the biological effect is mainly determined by the linear part (first additive term in equation (13)) of the biological effect (Kamp *et al* 2014). Therefore, we suggest that covariance elements (i.e. $j \neq m$) in $\Upsilon_{ijim}^{x/y}$ and $\Xi_{ijim}^{\sqrt{\beta}}$ can be neglected for a first approximation in the calculation of $\mathbb{E}[\varepsilon_i]$. This reduces the number of computations and can be interpreted as neglecting the influence of the interdependence of $L_{ij/im}^{x/y}$, $Z_{ij/im}^{\sqrt{\beta}}$ on the quadratic term of the expectation value of the biological effect $\mathbb{E}[\varepsilon_i]$. As a result, the second raw moments $\Upsilon_{ijim}^{x/y}$, and $\Xi_{ijim}^{\sqrt{\beta}}$ are approximated by squaring the first raw moments $\mathcal{L}_{ij}^{x/y}$, $\mathcal{Z}_{ij}^{\sqrt{\beta}}$, which corresponds to only considering the trace ($j = m$) of $\Upsilon_{ijim}^{x/y}$ and $\Xi_{ijim}^{\sqrt{\beta}}$. Through this formulation, the full analytical calculation of $\mathbb{E}[\varepsilon_i]$ in equation (13) can be approximated with $\hat{\mathbb{E}}[\varepsilon_i]$ in equation (14) and has then the same computational complexity as the calculation of the nominal biological effect according to equation (7):

$$\hat{\mathbb{E}}[\varepsilon_i] = \sum_{j}^{B} w_j \mathcal{L}_{ij}^{x} \mathcal{L}_{ij}^{y} \mathcal{Z}_{ij}^{\alpha} + \left(\sum_{j}^{B} w_j \mathcal{L}_{ij}^{x} \mathcal{L}_{ij}^{y} \mathcal{Z}_{ij}^{\sqrt{\beta}} \right)^2 = \sum_{j}^{B} w_j \mathcal{A}_{ij} + \left(\sum_{j}^{B} w_j \mathcal{B}_{ij} \right)^2. \tag{14}$$

Assessing the expectation value of the biological effect $\hat{\mathbb{E}}[\boldsymbol{\varepsilon}]$ reduces to computations of $\mathcal{L}_{ij}^{x/y}$ and $\mathcal{Z}_{ij}^{\alpha/\sqrt{\beta}}$ according to equations (B.2) and (B.3), respectively. For optimization, these quantities are stored in influence matrices $\mathcal{A} = \mathbb{E}[A]$ and $\mathcal{B} = \mathbb{E}[B]$ facilitating a linear-quadratic mapping for pencil beam weights to the expected biological effect.

2.4. Covariance of biological effect

The calculation of the covariance of the biological effect Σ^{ε} requires the evaluation of mixed terms $\mathbb{E}[\varepsilon_i \varepsilon_l]$

$$\Sigma^{\varepsilon}[\varepsilon_i, \varepsilon_l] = \mathbb{E}[\varepsilon_i \varepsilon_l] - \mathbb{E}[\varepsilon_i]\,\mathbb{E}[\varepsilon_l]. \tag{15}$$

Given the voxel indices i, l, the pencil beam indices j, m, o, q and let V be the number of voxels, B be the number of pencil beams, mixed terms then take the form

$$\begin{aligned}\mathbb{E}[\varepsilon_i\varepsilon_l] &= \int \mathrm{d}\boldsymbol{\Delta}^x\mathrm{d}\boldsymbol{\Delta}^y\mathrm{d}\boldsymbol{\Delta}^z p(\boldsymbol{\Delta}^x)\,p(\boldsymbol{\Delta}^y)\,p(\boldsymbol{\Delta}^z)\,p(\boldsymbol{\Delta}^z)\varepsilon_i(\boldsymbol{\Delta}^x,\boldsymbol{\Delta}^y,\boldsymbol{\Delta}^z)\varepsilon_l(\boldsymbol{\Delta}^x,\boldsymbol{\Delta}^y,\boldsymbol{\Delta}^z)\\ &= \sum_{jm}^{B} w_j w_m \Upsilon^x_{ijlm}\Upsilon^y_{ijlm}\Xi^{\alpha}_{ijlm} + 2\sum_{jmo}^{B} w_j w_m w_o \Upsilon^x_{ijlmio}\Upsilon^y_{ijlmio}\Xi^{\alpha 2\sqrt{\beta}}_{ijlmio}\\ &\quad + \sum_{jmoq}^{B} w_j w_m w_o w_q \Upsilon^x_{ijiolmlq}\Upsilon^y_{ijiolmlq}\Xi^{\sqrt{\beta}}_{ijiolmlq}. \end{aligned} \tag{16}$$

The derivation of equation (16) and a description of the calculations of the 6th order $\Xi^{\alpha 2\sqrt{\beta}}_{ijlmio}$ and 8th order $\Xi^{8\mathrm{th}\sqrt{\beta}}_{ijiolmlq}$ terms can be found in appendix C. As we are interested in the variance of the biological effect, which is stored in the diagonal of the covariance matrix $\Sigma^{\varepsilon}[\varepsilon_i,\varepsilon_l]$, we can explicitly drop additional voxel indices l and equation (16) can be reformulated to obtain:

$$\begin{aligned}\mathbb{E}[\varepsilon_i\varepsilon_i] &= \sum_{jm}^{B} w_j w_m \Upsilon^x_{ijm}\Upsilon^y_{ijm}\Xi^{\alpha}_{ijm} + 2\sum_{jmo}^{B} w_j w_m w_o \Upsilon^x_{ijmo}\Upsilon^y_{ijmo}\Xi^{\alpha 2\sqrt{\beta}}_{ijmo}\\ &\quad + \sum_{jmoq}^{B} w_j w_m w_o w_q \Upsilon^x_{ijmoq}\Upsilon^y_{ijmoq}\Xi^{\sqrt{\beta}}_{ijmoq}. \end{aligned} \tag{17}$$

Elements of these tensors correspond then to 2D (e.g. Υ^x_{ijm}), 3D (e.g. Υ^x_{ijmo}) and 4D (e.g. Υ^x_{ijmoq}) Gaussian distributions which are the results of integration over a bivariate, trivariate and quadvariate Gaussian distribution. Components in the first additive term (e.g. Υ^x_{ijm}) are in $\mathbb{R}^{V\times B^2}$, which would result for a typical clinical scenario with 10^6 voxels and $2\cdot 10^4$ pencil beams in $10^6\times 2\cdot 10^4\times 2\cdot 10^4 = 4\cdot 10^{14}$ tensor elements. Components in the second additive term (e.g. Υ^x_{ijmo}) are in $\mathbb{R}^{V\times B^3}$ and quantities in the third additive term (e.g. Υ^x_{ijmoq}) are in order $\mathbb{R}^{V\times B^4}$. These terms represent the second, third and fourth raw moment of the lateral/depth components $L^{x/y}, Z^{\alpha}, Z^{\sqrt{\beta}}$ in voxel i. Calculation of these high-dimensional tensors is associated with prohibitive computational complexity in a clinical setting.

Consequently, we propose exactly the same approximation as exercised previously for the calculation of the expectation value of the biological effect and neglect all covariance terms of different pencil beams emerging from $\sqrt{\boldsymbol{\beta}^{\boldsymbol{c}}}\circ\boldsymbol{d}$ terms. As the linear term $\boldsymbol{\alpha}^{\boldsymbol{c}}\circ\boldsymbol{d}$ of the biological effect dominates compared to the squared term $(\sqrt{\boldsymbol{\beta}^{\boldsymbol{c}}}\circ\boldsymbol{d})^2$ the contribution to the biological effect in the case of fraction doses, terms that are quadratic, cubic or even quadric in $\sqrt{\boldsymbol{\beta}^{\boldsymbol{c}}}\circ\boldsymbol{d}$ only correspond to a minor correction of the overall computation. Hence, tensors like $\Xi^{\alpha 2\sqrt{\beta^c}}_{ijmo}$ and $\Xi^{8\mathrm{th}\sqrt{\beta^c}}_{ijmoq}$ containing the $\sqrt{\boldsymbol{\beta}^{\boldsymbol{c}}}\circ\boldsymbol{d}$ dose term have decaying contributions from terms of higher order. Neglecting the covariance in terms containing $\sqrt{\boldsymbol{\beta}^{\boldsymbol{c}}}\circ\boldsymbol{d}$ then yields an approximation of the mixed term:

$$\begin{aligned}\hat{\mathbb{E}}[\varepsilon_i\varepsilon_i] &= \sum_{jm}^{B} w_j w_m \Upsilon^x_{ijm}\Upsilon^y_{ijm}\Xi^{\alpha}_{ijm} + 2\sum_{jmo}^{B} w_j w_m w_o \Upsilon^x_{ijm}\mathcal{L}^x_{io}\,\Upsilon^y_{ijm}\mathcal{L}^y_{io}\,\mathcal{Z}^{\alpha}_{ij}\mathcal{Z}^{\sqrt{\beta}}_{im}\mathcal{Z}^{\sqrt{\beta}}_{io}\\ &\quad + \sum_{jm}^{B} w_j w_m (\Upsilon^x_{ijm})^2(\Upsilon^z_{ijm})^2(\mathcal{Z}^{\sqrt{\beta}}_{ij}\mathcal{Z}^{\sqrt{\beta}}_{im})^2\\ &= \sum_{jm}^{B} w_j w_m \hat{\mathfrak{D}}^{\varepsilon}_{ijm} \end{aligned} \tag{18}$$

where $\hat{\mathfrak{D}}^{\varepsilon}_{ijm}$ denotes the trace of the full variance influence tensor $\hat{\mathfrak{D}}^{\varepsilon}_{ijlm}$. The last step of equation (18) collapses the sum for w_o in the second term to reduce the dimensionality for further consideration. Herewith, the integration over trivariate Gaussian distributions factorizes into the integration over univariate and bivariate Gaussian distributions. Analogous, the integration over quadvariate Gaussian distributions is represented by the product of two integrated bivariate Gaussian distributions. This reduces the computational complexity and storage requirements for the second raw moment of the probability distribution of the biological effect from $\mathcal{O}(V \times B^4)$ to $\mathcal{O}(V \times B^2)$. Substituting (18) in (15) yields the second central moment of the biological effect:

$$\begin{aligned}\hat{\sigma}^2[\varepsilon_i] = \hat{\Sigma}^{\varepsilon}[\varepsilon_i, \varepsilon_i] = \hat{\mathbb{E}}[\varepsilon_i \varepsilon_i] - \hat{\mathbb{E}}[\varepsilon_i]\,\hat{\mathbb{E}}[\varepsilon_i] = \sum_{jm}^{B} w_j w_m \mathfrak{V}^{\varepsilon}_{ijm} \\ = \sum_{jm}^{B} \left(w_j w_m \hat{\mathfrak{D}}^{\varepsilon}_{ijm} - \left[\mathcal{A}_{ij} w_j + (\mathcal{B}_{ij} w_j)^2\right]\left[\mathcal{A}_{im} w_m + (\mathcal{B}_{im} w_m)^2\right]\right).\end{aligned} \tag{19}$$

Besides higher storage requirements and the two to threefold increased numerical computations required for biological treatment planning in relation to treatment planning based on the physical dose, the complexity of the approximated variance calculation of the biological effect equals the complexity of the variance of the physical dose. If not stated otherwise, calculations of the expectation value and variance of the biological effect are, for the remainder of this paper, based on the approximations shown in equations (14) and (18).

2.5. Probabilistic optimization of the biological effect

The expectation value $\mathbb{E}[\varepsilon]$ and the covariance Σ^{ε} of the biological effect together constitute a Gaussian approximation of the probability density of the biological effect:

$$p(\varepsilon) = \mathcal{N}\left(\varepsilon, \mathbb{E}[\varepsilon], \Sigma^{\varepsilon}\right). \tag{20}$$

This representation enables a probabilistic optimization using a piece-wise quadratic objective function according to Unkelbach and Oelfke (2004) and Bangert *et al* (2013). With the diagonal penalty matrix $P = \mathrm{diag}(p_1, p_2, ..., p_N)$ and the prescribed biological effect ε^*, the expected value of the piece-wise quadratic objective function is given by

$$\mathbb{E}[\mathcal{F}] = \mathrm{tr}(P\Sigma^{\varepsilon}) + \left(\mathbb{E}[\varepsilon] - \varepsilon^*\right)^T P \left(\mathbb{E}[\varepsilon] - \varepsilon^*\right) \tag{21}$$

which can be evaluated very efficiently during optimization (Bangert *et al* 2013, Wahl *et al* 2017).

2.6. Nonlinear conversion of moments of the biological effect to moments of the RBE-weighted dose

Clinical decision making and treatment plan evaluation in carbon ion therapy are usually based on the RBE-weighted dose. For this reason, the expectation value and variance of the biological effect are converted to the expectation value and variance of the RBE-weighted dose using a Taylor expansion, a commonly known error- or uncertainty propagation method. In particular, a fourth order Taylor expansion at $\mathbb{E}[\varepsilon_i]$ evaluating partial derivatives at ε_i is employed to approximate the nonlinear conversion of moments of the biological effect (Anderson and

Table 1. Information regarding the three different patient cases and their corresponding plan parameters. The third row 'lat. spot distance' denotes the lateral spot spacing in the isocenter plane and # voxels σ depicts the number of voxels for which standard deviation was calculated. The number of pencil beams and the number of voxels for σ calculation are the dominant factors for the overall runtime.

	Unit	Intra-cranial	Para-spinal	Prostate
Gantry angles	(°)	50°, 135°	135°, 180°, 225°	90°, 180°
Couch angles	(°)	0°, 0°	0°, 0°, 0°	0°, 0°
Lat. spot distance	(mm)	3	4	5
Resolution	(mm^3)	$(1.2 \times 1.2 \times 3)$	$(3 \times 3 \times 3)$	$(2 \times 2 \times 3)$
# pencil beam	—	2022	17 756	15 669
# voxels σ	—	0.95×10^5	1.2×10^5	0.83×10^5
# fractions f	—	1	5	20
Pres. fraction dose	(Gy(RBE))	3	3	3

Mattson 2012). The nonlinearity is brought in by the square root of a scaled version of the biological effect in equation (1). Given $\gamma = \frac{\alpha_x}{2\beta_x}$, the propagation of moments then takes the following form:

$$\mathbb{E}[\text{RBE} \times d_i] \approx \sqrt{\beta_x^{-1}\mathbb{E}[\varepsilon_i] + \gamma^2} - \gamma - \frac{\beta_x^{-2}}{8(\beta_x^{-1}\mathbb{E}[\varepsilon_i] + \gamma^2)^{\frac{3}{2}}}\sigma[\varepsilon_i]^2 - \frac{5\beta_x^{-4}}{128(\beta_x^{-1}\mathbb{E}[\varepsilon_i] + \gamma^2)^{\frac{7}{2}}}\sigma[\varepsilon_i]^2 \tag{22}$$

$$\sigma[\text{RBE} \times d_i]^2 \approx \frac{\beta_x^{-1}}{2(\beta_x^{-1}\mathbb{E}[\varepsilon_i] + \gamma^2)^{\frac{1}{2}}}\sigma[\varepsilon_i]^2 + \frac{1}{2}\left(\frac{\beta_x^{-2}}{8(\beta_x^{-1}\mathbb{E}[\varepsilon_i] + \gamma^2)^{\frac{3}{2}}}\right)^2 \sigma[\varepsilon_i]^4. \tag{23}$$

The Taylor expansion around ε_i is only locally valid, meaning the approximation quality generally shrinks when the variance of the biological effect increases. Furthermore, potential deviation from the Gaussian form (e.g. skewness or bimodal distributions) that is not captured by a simple two variable model may compromise error propagation.

2.7. Validation

The accuracy of the proposed analytical approximations for the expectation value and variance of the biological effect was investigated on a simplified artificial example in section 3.1. A 1D carbon ion SOBP with 150 mm range and 50 mm modulation was investigated considering 3.5% range uncertainty. The SOBP was optimized performing an effect-based optimization according to Wilkens and Oelfke (2006). The resulting probabilistic quantities are compared against sampled references in terms of maximal deviation.

As the approximations closely match the sampled values, we demonstrate the use of APM for carbon ions in three concrete clinical settings in section 3.2. Specifically, we evaluated the APM formalism in a treatment planning study using conventional and probabilistic optimization considering setup-, range-errors and fractionation effects. Information regarding uncertainty assumptions is given in section 2.2 and details of the patient cases and treatment plan parameters can be found in table 1.

For each case, we investigated the accuracy of APM moment computations for carbon ions in comparison to random sampling for unfractionated treatment (fraction $f = 1$). The objective function applied for treatment planning features squared deviation objectives with a prescribed fraction dose of 3 Gy(RBE) for the CTV and squared overdosing objectives for the outer contour and critical structures. We perform both conventional optimization and probabilistic optimization according to equation (21). 3D γ-pass rates according to Low *et al* (1998), utilizing a distance to agreement of 2 mm and a dose difference criterion of 2%, were used for the evaluation.

Both the 1D SOBP as well as the patient cases are compared against sampled references. Using 5000 samples ensures that the standard error of the sampled mean $\sigma[\mathbb{E}[\varepsilon]]$ falls below 1.4% and the expected relative error of the standard deviation $\sigma[\sigma[\varepsilon]]$ drops below 1% (Squires 2001).

For a proof of principle, the moment computations for carbon ions were implemented in matRad, an open-source treatment planning toolkit (Wieser *et al* 2017), which is entirely written in the numerical computation environment Matlab (2016b, The MathWorks Inc).

All results presented in this paper are based on photon reference radio-sensitivity parameters $\alpha_x = 0.1\,\mathrm{Gy}^{-1}$ and $\beta_x = 0.05\,\mathrm{Gy}^{-2}$. We assumed a single biological system and assigned these tissue specific parameters to all patient voxles.

3. Results

3.1. Uncertainty quantification of a 1D SOBP

The 1D carbon ion SOBP is shown in figure 2(a) and was computed according to equation (9). Figure 2(b) considers the same SOBP, however, with 3.5% range uncertainty.

Figure 2(b) compares the full analytical computation $\mathbb{E}[\varepsilon]$, its approximation $\hat{\mathbb{E}}[\varepsilon]$ and sampled references of the expected biological effect. The individual terms $\mathcal{Z}^{\alpha}\boldsymbol{w}$ and $(\mathcal{Z}^{\sqrt{\beta}}\boldsymbol{w})^2$ contributing to the approximated expectation value of the biological effect $\hat{\mathbb{E}}[\varepsilon]$ according to equation (14) are also shown. Figure 2(c) explicitly visualizes the quality of the approximation for $(\mathcal{Z}^{\sqrt{\beta}}\boldsymbol{w})^2$ against the full analytical calculation $\boldsymbol{w}^T\Xi^{\sqrt{\beta}}\boldsymbol{w}$. As the maximum difference between the full analytical expected biological effect $\mathbb{E}[\varepsilon]$ based on equation (12) and the approximated expected biological effect $\hat{\mathbb{E}}[\varepsilon]$ introduced in equation (14) amounts only to 0.18%, we use the latter for further consideration. The maximum difference of the expected biological effect $\mathbb{E}[\varepsilon]$ based on sampling (shown by green crosses in figure 2(b)) to the full analytical calculation of the biological effects using 5000 samples is 0.39 %.

Figure 3 shows the variance calculation of the biological effect as laid out in section 2.4. Discrepancies between $\hat{\sigma}[\varepsilon]$ and the sampled standard deviation were caused by neglecting correlations in $\sqrt{\boldsymbol{\beta}^{\boldsymbol{c}}} \circ \boldsymbol{d}$ but did not exceed 5.2%; the root mean squared error was 0.002 (ε is a dimensionless quantity). One way to increase the accuracy of the standard deviation of the biological effect was to additionally consider covariance elements in the second additive term in equation (17). Doing so reduced the maximum relative deviation to 2.3% and the RMSE to 0.0016%. Finally, a full analytical calculation of $\sigma[\varepsilon]$ based on equation (17) further lowered the maximum relative deviation to 0.9%.

The histogram on the vertical axis in figure 3 shows the actual distribution of the biological effect of a single voxel at depth $z = 150$ mm obtained by means of sampling. As this voxel is located at the distal fall off of the SOBP, small range shifts result either in a biological effect of $\sim$0.75 (high-effect) or $\sim$0.1 (low-effect region). This behaviour is reflected by the bimodal-shaped probability distribution with peaks at $\sim$0.75 and $\sim$0.1. For subsequent error

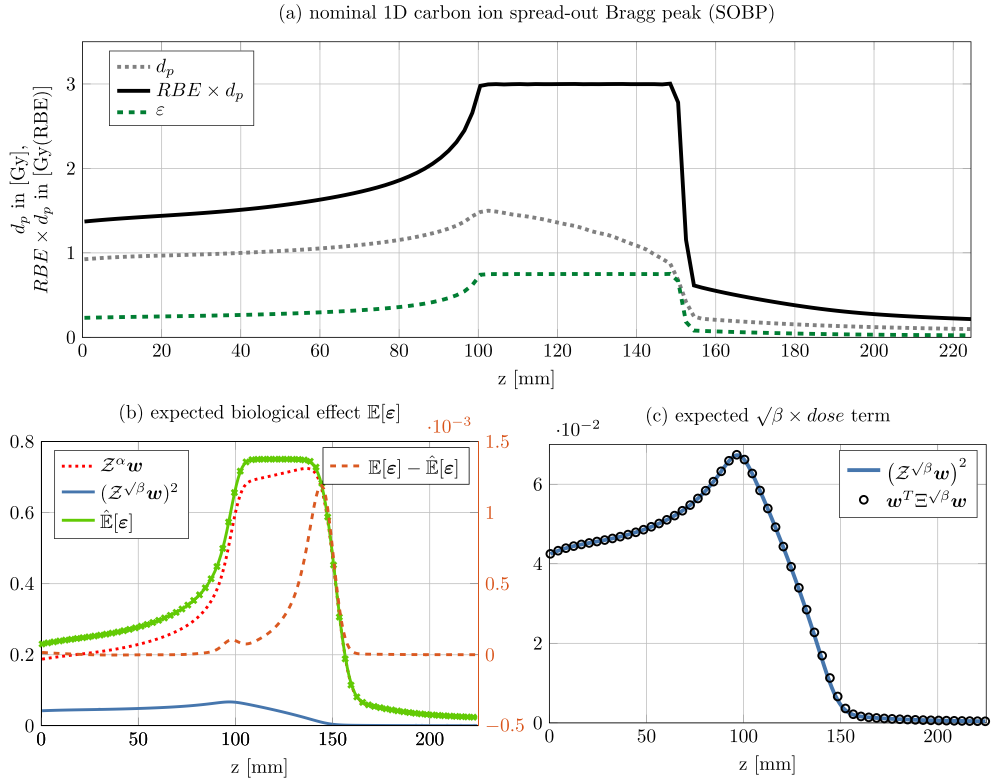

Figure 2. (a) Nominal physical dose d_p, RBE-weighted dose RBE $\times$ d_p, and biological effect ε of a 1D carbon ion SOBP with range 150 mm and 50 mm modulation. Calculations are based on photon radio-sensitivity parameters $\alpha_x = 0.1$ Gy^{-1} and $\beta_x = 0.05$ Gy^{-2}. The prescribed target dose is 3 Gy(RBE). (b) Approximated expected biological effect $\hat{\mathbb{E}}[\varepsilon]$ (solid green) and its components (solid blue and dotted red) considering a range uncertainty of 3.5%. The difference between approximate and full expected biological effect calculation is shown in dashed orange (note the different scale on the right). Additionally, the expected biological effect from 5000 sampling experiments is shown by green crosses. (c) The differences of the proposed approximation (solid blue line) to the full analytical calculation (black circles) of the term $(\mathcal{Z}^{\sqrt{\beta}}\boldsymbol{w})^2$. Note that the blue solid lines in figures 2(b) and (c) are the same.

propagation into RBE-weighted dose, however, we use a Gaussian probability density (solid black line on the vertical axis) as we only calculate analytically the expectation value and standard deviation of the unknown probability distribution of the biological effect.

3.2. Application of APM on patient cases

Resulting $\hat{\mathbb{E}}[\text{RBE} \times d_p]$—and $\hat{\sigma}[\text{RBE} \times d_p]$ distributions based on conventional- and probabilistic-optimization for the transversal iso-center slices for all three patient cases are shown in figure 4, whereas $\hat{\mathbb{E}}[\text{RBE} \times d_p]$- and $\hat{\sigma}[\text{RBE} \times d_p]$ were established according to the approximated analytical probabilistic modeling pipeline in section 2.

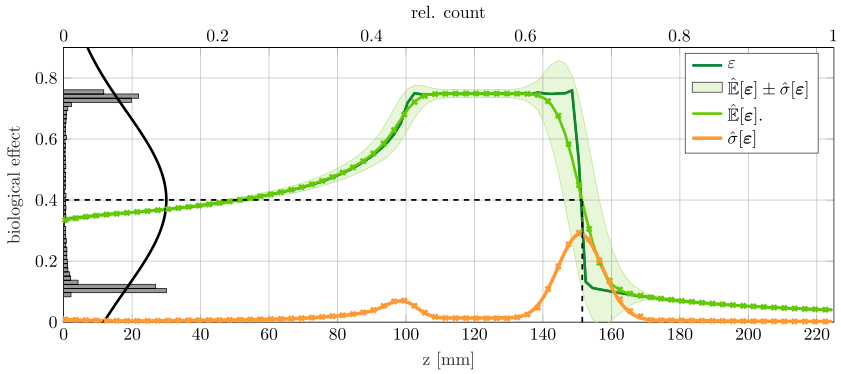

Figure 3. Biological effect of a 1D C12 SOBP. The dark green solid line represents the nominal biological effect ε. The bright green solid line visualizes the expected biological effect $\hat{\mathbb{E}}[\varepsilon]$ considering 3.5% range uncertainty. The orange solid line depicts the approximated standard deviation of the biological effect $\hat{\sigma}[\varepsilon]$. Crosses indicate sampling results ($N = 5000$). The histogram on the y axis visualizes the probability distribution of the biological effect for $z = 150$ mm. Gaussian approximation based on the computed expectation value and variance (solid black) does not capture the bimodal distribution of the biological effect in high variance regions.

Similar to previous reports on probabilistic optimization with protons (Unkelbach *et al* 2009) and worst case optimization with carbon ions (Steitz *et al* 2016), APM creates a high dose margin around the CTV resulting in a reduced standard deviation inside the CTV while at the same time lowering the standard deviation within the organs at risk. This phenomenon is also reflected in the corresponding standard deviation volume histogram in figure 5(a). Similar results are observed for the other patient cases considering different fractionation schemes (figures 5(b) and (c)).

Calculation times for a complete clinical work-flow, including the calculation of the expectation value and standard deviation of the RBE-weighted dose as well as a probabilistic optimization, ranged between 4 and 7 h for individual patient cases using a regular desktop machine[4].

3D γ-pass rates according to Low *et al* (1998), utilizing a distance to agreement of 2 mm and a dose difference criterion of 2%, were calculated and are shown in table 2. Results have to be interpreted with caution because random sampling is subject to uncertainty. Nevertheless, there is a good match between the approximated analytical and sampling based quantities, therefore justifying the approximations made in sections 2.3 and 2.4 to assess $\hat{\mathbb{E}}[\varepsilon]$ and $\hat{\sigma}[\varepsilon]$. The decrease of the γ-pass rates from $\hat{\mathbb{E}}[\varepsilon]$ and $\hat{\sigma}[\varepsilon]$ to $\hat{\mathbb{E}}[\mathrm{RBE} \times d_p]$ and $\hat{\sigma}[\mathrm{RBE} \times d_p]$ can be attributed to inaccuracies in the error propagation (see section 2.6). All γ-pass rates comparing approximated analytical and sampled quantities are above 94.95%.

Figure 5 depicts the standard deviation volume histograms of all patient cases, thereby explicitly comparing the results obtained via conventional optimization (no robustness considered) and probabilistic optimization (robustness consideration). The standard deviation histograms, which provide comprehensive information regarding the dose uncertainty within a specific volume of interest, are in agreement with the single slice displays of the standard deviation in figure 4.

[4] macOS Sierra, 2.7 GHz Intel Core i7, 16GB 2133 MHz RAM.

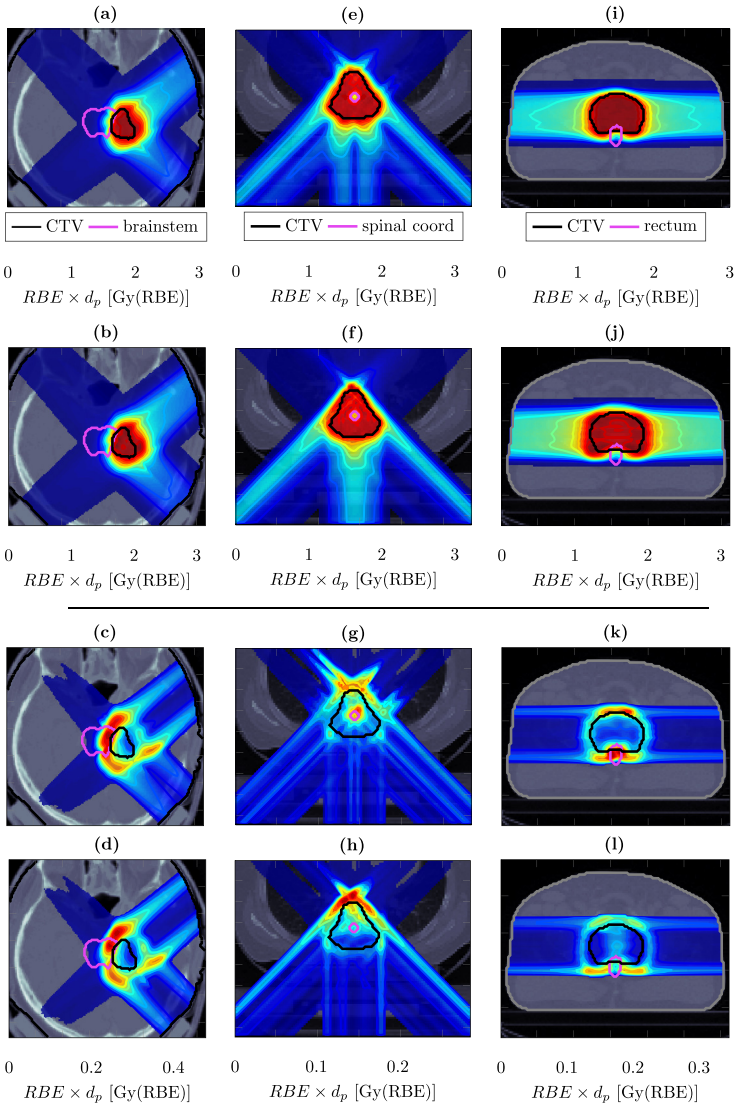

Figure 4. Transversal slices of intensity-modulated carbon ion therapy treatment plans defined in table 1 assuming a different number of fractions. The CT data is superimposed with transparent dose colorwash, solid iso-dose lines, and contours of volumes of interest. Figures (a)–(d) refer to an intra-cranial case, (e)–(h) to a para-spinal case and (i)–(l) to a prostate case. The expectation value and standard deviation of the RBE-weighted dose based on a conventional optimization (labeled 'conv.opt.') are shown in the first and third row. Figures in the second and fourth row marked with 'prop.opt.' depict the results obtained from probabilistic optimization. (a) $\hat{\mathbb{E}}[\text{RBE} \times d_p]$ conv.opt. (b) $\hat{\mathbb{E}}[\text{RBE} \times d_p]$ prop.opt. (c) $\hat{\sigma}[\text{RBE} \times d_p]$ conv.opt. (d) $\hat{\sigma}[\text{RBE} \times d_p]$ prop. opt. (e) $\hat{\mathbb{E}}[\text{RBE} \times d_p]$ conv.opt. (f) $\hat{\mathbb{E}}[\text{RBE} \times d_p]$ prob.opt. (g) $\hat{\sigma}[\text{RBE} \times d_p]$ conv.opt. (h) $\hat{\sigma}[\text{RBE} \times d_p]$ prob.opt. (i) $\hat{\mathbb{E}}[\text{RBE} \times d_p]$ conv.opt. (j) $\hat{\mathbb{E}}[\text{RBE} \times d_p]$ prob.opt. (k) $\hat{\sigma}[\text{RBE} \times d_p]$ conv.opt. (l) $\hat{\sigma}[\text{RBE} \times d_p]$ prob.opt.

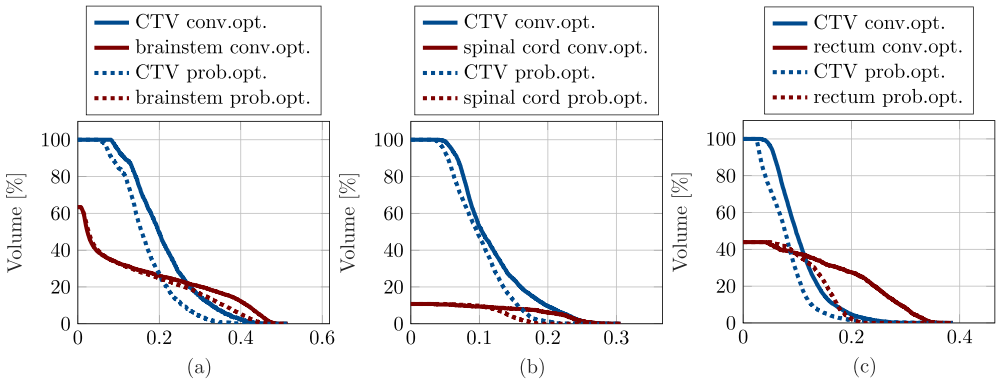

Figure 5. Standard deviation volume histograms of the RBE-weighted dose for the (a) intra-cranial case assuming 1 fraction, (b) the para-spinal case assuming 5 fractions, and (c) the prostate case optimized for 30 fractions. Solid lines represent the results obtained from conventional optimization (conv.opt.) and dashed lines are based on probabilistic APM optimization (prob.opt.). (a) $\hat{\sigma}[\mathrm{RBE} \times D]$ [Gy(RBE)]. (b) $\hat{\sigma}[\mathrm{RBE} \times D]$ [Gy(RBE)]. (c) $\hat{\sigma}[\mathrm{RBE} \times D]$ [Gy(RBE)].

4. Discussion

We demonstrated the feasibility of analytical computations of the expected value and variance of the biological effect and RBE-weighted dose in intensity-modulated carbon ion therapy considering setup and range uncertainties. The entire analytical pipeline for carbon ion therapy maintains compatibility with APM's core advantages allowing for (i) multi-dimensional linearly correlated random input variables, (ii) the definition of arbitrary correlation models, (iii) subsequent probabilistic optimization.

We decided to build APM upon the biological effect to avoid integrating equation (1) with the square root dependence against Gaussian densities. Besides analytical solutions, we introduced analytical approximations which effectively reduce the number of operations (i) for the expected biological effect from $\mathcal{O}(V \times B^2)$ to $\mathcal{O}(V \times B)$ and (ii) for the variance of the biological effect from $\mathcal{O}(V \times B^4)$ to $\mathcal{O}(V \times B^2)$ both at marginal loss in accuracy. We want to point out that the observed discrepancies between APM computations and 5000 samples for $\hat{\mathbb{E}}[\varepsilon]$ and $\hat{\sigma}[\varepsilon]$ are not only related to the approximations within the APM formalism but are also due to residual statistical uncertainty in the sampling based reference. Furthermore, we demonstrated on three patient cases that APM can effectively be used for uncertainty minimization through probabilistic optimization of the biological effect.

The calculation of the expected biological effect exhibits the same computational complexity as the nominal biological effect $\mathcal{O}(V \times B)$; assessing its variance using the proposed method requires $\mathcal{O}(V \times B^2)$ operations. Consequently, the most time critical treatment plan parameters are the pencil beam grid spacing and the number of pencil beam contributions to voxel i. Despite the fact that carbon ions exhibit $\sim$3 times less lateral scattering compared to protons, the number of dose deposition points is usually higher for carbon ions due to the fragmentation tail. For this reason, APM calculation times for carbon ions are in general longer compared to protons. Our current prototype implementation in the interpreted programming language Matlab still requires comparably long computations (4–7 h per patient case). To increase runtime, an implementation in our C++ based in-house treatment planning system built upon the MITK framework (Wolf *et al* 2005) is part of ongoing work. In general, we

Table 2. Global γ-pass rates for the expectation value and standard deviation of the biological effect and RBE-weighted dose on the basis of analytical calculations and random sampling (5000 samples). Three patient cases are under investigation considering one fraction. The abbreviation 'conv.opt.' indicates conventional optimization whereas 'prob.opt.' denotes probabilistic optimization. A distance to agreement of 2 mm and a dose difference criteria of 2% were used for the γ-analysis.

Case	Resolution (mm)	conv.opt.		prob.opt.	
		$\mathbb{E}[\varepsilon]$ (%)	$\sigma[\varepsilon]$ (%)	$\mathbb{E}[\varepsilon]$ (%)	$\sigma[\varepsilon]$ (%)
Intra-cranial	$1.1 \times 1.1 \times 3$	100	99.88	100	99.82
Paraspinal	$3 \times 3 \times 3$	99.71	97.56	99.98	98.30
Prostate	$3 \times 3 \times 3$	100	99.41	99.49	98.70
		$\mathbb{E}[\text{RBE} \times d_p]$ (%)	$\sigma[\text{RBE} \times d_p]$ (%)	$\mathbb{E}[\text{RBE} \times d_p]$ (%)	$\sigma[\text{RBE} \times D]$ (%)
Intra-cranial	$1.1 \times 1.1 \times 3$	100	98.82	100	99.44
Paraspinal	$3 \times 3 \times 3$	99.99	94.95	99.15	96.28
Prostate	$3 \times 3 \times 3$	100	98.76	97.63	97.56

expect a similar relative performance for carbon ions as for protons where we have already shown that APM enables effective uncertainty quantification and probabilistic treatment plan optimization for protons using a constant RBE with total runtimes of a few minutes using our C++ in-house treatment planning system on regular desktop machines (Wahl *et al* 2017). In particular, it could be established that APM generally exhibits a better trade-off between speed and accuracy compared to sampling-based uncertainty quantification and minimization—especially in the context of fractionated radiation therapy (Wahl *et al* 2017).

In contrast to the work based on the same APM concept presented in Bangert *et al* (2013) and Wahl *et al* (2017), who modeled the impact of physical uncertainties on the physical dose, this work is about the impact of physical uncertainties on the biological effect considering a variable RBE and the correlation between physical and biological beam properties. A direct application of the physical dose-based formalism presented by Bangert *et al* (2013) and Wahl *et al* (2017) to carbon ion treatment planning is not suitable as it does not model the dependence of RBE on the particle spectra, tissue type and dose level.

Although we observe a maximal discrepancy of 5.2% comparing the approximated variance against sampled references for the 1D SOBP, we argue that this discrepancy is mitigated in a clinical 3D treatment plan for two reasons: (i) we usually do not see such steep dose gradients, and (ii) a lateral neighboring pencil beam will also have an influence and will consequently lower the variance.

The nonlinear propagation of moments of the biological effect to moments of the RBE-weighted dose is achieved via a Taylor expansion around $\mathbb{E}[\varepsilon]$. Although the distribution over the biological effect is non-Gaussian and the RBE-weighted dose computation itself is nonlinear, the error propagation only slightly diminishes the accuracy of APM calculations against random sampling results (see table 2). Calculating higher order moments $n > 2$ (skewness and kurtosis) of the biological effect would, in principle, permit a more precise shape description of the unknown probability distribution of the biological effect ε_i in voxel i.

Throughout this work, the lateral dose was only modeled by a single Gaussian component which might not model the low-dose halo accurately enough. In general, our considerations also apply to double or triple Gaussian lateral beam models. Similar to the depth components, the lateral dose could then also be modelled with a superposition of Gaussians.

Setup and range uncertainties are modelled in this article by multivariate normal distributions. Whilst it is common practice to describe uncertainties in the context of radiotherapy with Gaussian probability densities, the APM framework also facilitates modeling uniform distribution or any arbitrary probability density by a superposition of Gaussians. The latter illustrates again the core concept of APM, which is the approximation of non-integrable functions by a set of easily integrable functions—in this case Gaussians—to solve equation (4) in closed-form.

We want to emphasize that we assumed a single biological system for treatment planning and did not assign different photon LQ model radio-sensitives to individual structures. But we want to point out that it is in principle possible to use different $\frac{\alpha_x}{\beta_x}$ ratios for different tissues in our approach if desired by the planner. As all results presented in this manuscript refer to photon LQ model parameter $\alpha_x = 0.1\ \mathrm{Gy}^{-1}$ and $\beta_x = 0.05\ \mathrm{Gy}^{-2}$, we also evaluated and concluded that the mathematical deviations and approximations also hold for $\alpha_x = 0.5\ \mathrm{Gy}^{-1}$ and $\beta_x = 0.05\ \mathrm{Gy}^{-2}$.

The approach presented in this paper is generally applicable to biological treatment planning using other ion species such as protons or helium ions, provided that dose-averaged particle radio-sensitivity curves are available for various initial beam energies. APM does not depend on the underlying biophysical model; it allows for the incorporation of biological base data from other biophysical or phenomenological models.

The radio-sensitivity parameters of heavier ions are subjected to pronounced uncertainties; however, their variability has never been taken into account during optimization. This work may be the basis to account for uncertainties in the particle α_p and β_p parameters of the LQ model. In particular, APM's capability to incorporate arbitrary correlation assumptions might be beneficial when modeling radio-sensitivity uncertainties (i) between α_p and β_p parameters, and (ii) along penetrated tissues for individual pencil beams. This would allow us to not only incorporate physical but also biological uncertainties into the treatment planning process of charged particles.

5. Conclusion

Using analytical probabilistic modeling, it is possible to calculate the expectation value and variance of RBE-weighted dose distributions in intensity-modulated scanned carbon ion therapy in closed-form considering setup and range errors including fractionation effects. Using low-rank approximations for the required tensor computations, it is possible to perform non-linear computations of the RBE-weighted dose at the same computational complexity as the linear computations of the physical dose with minimal loss of accuracy. We compare APM moment calculations for three patient cases against sampling-based references and observe global γ-pass rates (2 mm, 2%) of >99.15% for the expectation value and >94.95% for the standard deviation of the RBE-weighted dose. All mathematical derivations for calculating the statistical moments of the biological effects maintain compatibility with APM's special features of (i) enabling multi-dimensional linearly correlated random input variables, (ii) modeling arbitrary correlations, and (iii) generalizing to probabilistic optimization.

Acknowledgments

We would like to thank the Probabilistic Numerics Group of the Max Planck Institute for Intelligent Systems in Tübingen for helpful discussions. Financial support from the German Research Foundation, Grant No. BA 2279/3-1, is gratefully acknowledged.

Appendix A. Analytical probabilistic modeling notation

Table A1. Notation used to describe APM for biological treatment planning.

Notation	Meaning	Description	Complexity
L	L	Lateral dose in x, y	$\mathcal{O}(V \times B)$
$\mathcal{L}$	$\mathbb{E}[L]$	1st central moment of lateral dose	$\mathcal{O}(V \times B)$
Υ	$\mathbb{E}[L^2]$	2nd central moment of lateral dose	$\mathcal{O}(V^2 \times B^2)$
Z	Z	Depth dose in z	$\mathcal{O}(V \times B)$
$\mathcal{Z}$	$\mathbb{E}[Z]$	1st central moment of depth dose	$\mathcal{O}(V \times B)$
Ξ	$\mathbb{E}[Z^2]$	2nd central moment of depth dose	$\mathcal{O}(V^2 \times B^2)$
D	$L^x L^y Z$	Dose influence matrix	$\mathcal{O}(V \times B)$
$\mathcal{D}$	$\mathbb{E}[D] = \mathcal{L}^x \mathcal{L}^y \mathcal{Z}$	Expected dose influence matrix	$\mathcal{O}(V \times B)$
$\mathfrak{D}$	$\mathbb{E}[D^2] = \Upsilon^x \Upsilon^y \Xi$	2nd central moment of dose influence matrix	$\mathcal{O}(V^2 \times B^2)$
$\mathfrak{V}$	$\Upsilon^x \Upsilon^y \Xi - \mathcal{D}^2$	Covariance influence tensor	$\mathcal{O}(V^2 \times B^2)$
Z^α	Z^α	Depth component $\alpha \circ d$ in z	$\mathcal{O}(V \times B)$
$\mathcal{Z}^\alpha$	$\mathbb{E}[Z^\alpha]$	1st central moment of depth $\alpha \circ d$	$\mathcal{O}(V \times B)$
Ξ^α	$\mathbb{E}[Z^{\alpha\,2}]$	2nd central moment of depth $\alpha \circ d$	$\mathcal{O}(V^2 \times B^2)$
$Z^{\sqrt{\beta}}$	$Z^{\sqrt{\beta}}$	Depth component $\sqrt{\beta} \circ d$	$\mathcal{O}(V \times B)$
$\mathcal{Z}^{\sqrt{\beta}}$	$\mathbb{E}[Z^{\sqrt{\beta}}]$	1st central moment of depth $\sqrt{\beta} \circ d$	$\mathcal{O}(V \times B)$
$\Xi^{\sqrt{\beta}}$	$\mathbb{E}[Z^{\sqrt{\beta}\,2}]$	2nd central moment of depth $\sqrt{\beta} \circ d$	$\mathcal{O}(V^2 \times B^2)$
A	$L^x L^y Z^\alpha$	Influence matrix of the linear term	$\mathcal{O}(V \times B)$
$\mathcal{A}$	$\mathbb{E}[A] = \mathcal{L}^x \mathcal{L}^y \mathcal{Z}^\alpha$	Expected linear term of bio. effect	$\mathcal{O}(V \times B)$
Ψ	$\mathbb{E}[A^2] = \Upsilon^x \Upsilon^y \Xi^\alpha$	2nd central moment of linear term of bio. effect	$\mathcal{O}(V^2 \times B^2)$
B	$L^x L^y Z^{\sqrt{\beta}}$	Influence matrix of the squared term	$\mathcal{O}(V \times B)$
$\mathcal{B}$	$\mathbb{E}[B] = \mathcal{L}^x \mathcal{L}^y \mathcal{Z}^{\sqrt{\beta}}$	Expected squared term of bio. effect	$\mathcal{O}(V \times B)$
Φ	$\mathbb{E}[B^2] = \Upsilon^x \Upsilon^y \Xi^{\sqrt{\beta}}$	2nd central moment of squared term of bio. effect	$\mathcal{O}(V^2 \times B^2)$
ε	$A\boldsymbol{w} + (B\boldsymbol{w})^2$	Biological effect	$\mathcal{O}(V \times B)$
$\mathbb{E}[\varepsilon]$	$\mathcal{A}\boldsymbol{w} + \boldsymbol{w}^T \Phi \boldsymbol{w}$	Expected bio. effect	$\mathcal{O}(V \times B^2)$
$\hat{\mathbb{E}}[\varepsilon]$	$\mathcal{A}\boldsymbol{w} + (\mathcal{B}\boldsymbol{w})^2$	Approx. expected bio. effect	$\mathcal{O}(V \times B)$
$\mathfrak{D}^\varepsilon$	—	2nd central moment of bio. effect	$\mathcal{O}(V^2 \times B^4)$
$\hat{\mathfrak{D}}^\varepsilon$	—	Approx. 2nd central moment of bio. effect	$\mathcal{O}(V^2 \times B^2)$
$\hat{\mathfrak{V}}^\varepsilon$	$\tilde{\mathfrak{D}}^\varepsilon - \hat{\mathbb{E}}[\varepsilon]^2$	Approx. covariance influence tensor of bio. effect	$\mathcal{O}(V^2 \times B^2)$

Appendix B. Calculation of expected biological effect

Let i, l be voxel indices, j, m be pencil beam indices and B be the number of pencil beams, then the full analytical calculation of the expectation value of the biological effect in voxel i

considering setup and range errors is given by:

$$\begin{aligned}
\mathbb{E}[\varepsilon_i] &= \int \mathrm{d}\boldsymbol{\Delta}^x \mathrm{d}\boldsymbol{\Delta}^y \mathrm{d}\boldsymbol{\Delta}^z\, p(\boldsymbol{\Delta}^x)\, p(\boldsymbol{\Delta}^y)\, p(\boldsymbol{\Delta}^z) \varepsilon_i(\boldsymbol{\Delta}^x, \boldsymbol{\Delta}^y, \boldsymbol{\Delta}^z) \\
&= \int \mathrm{d}\boldsymbol{\Delta}^x \mathrm{d}\boldsymbol{\Delta}^y \mathrm{d}\boldsymbol{\Delta}^z\, p(\boldsymbol{\Delta}^x)\, p(\boldsymbol{\Delta}^y)\, p(\boldsymbol{\Delta}^z) \left[\sum_j^B w_j L_{ij}^x L_{ij}^y Z_{ij}^\alpha + \left(\sum_j^B w_j L_{ij}^x L_{ij}^y Z_{ij}^{\sqrt{\beta}} \right)^2 \right] \\
&= \sum_j^B w_j \left\{ \int \mathrm{d}\boldsymbol{\Delta}^x p(\boldsymbol{\Delta}^x) L_{ij}^x \right\} \left\{ \int \mathrm{d}\boldsymbol{\Delta}^y p(\boldsymbol{\Delta}^y) L_{ij}^y \right\} \left\{ \int \mathrm{d}\boldsymbol{\Delta}^z p(\boldsymbol{\Delta}^z) Z_{ij}^\alpha \right\} \\
&\quad + \sum_{jm}^B w_j w_m \left\{ \int \mathrm{d}\boldsymbol{\Delta}^x p(\boldsymbol{\Delta}^x) L_{ij}^x L_{im}^x \right\} \left\{ \int \mathrm{d}\boldsymbol{\Delta}^y p(\boldsymbol{\Delta}^y) L_{ij}^y L_{im}^y \right\} \\
&\quad \left\{ \int \mathrm{d}\boldsymbol{\Delta}^z p(\boldsymbol{\Delta}^z) Z_{ij}^{\sqrt{\beta}} Z_{im}^{\sqrt{\beta}} \right\} \\
&= \sum_j^B w_j \mathcal{L}_{ij}^x \mathcal{L}_{ij}^y \mathcal{Z}_{ij}^\alpha + \sum_{jm}^B w_j w_m \Upsilon_{ijim}^x \Upsilon_{ijim}^y \Xi_{ijim}^{\sqrt{\beta}}.
\end{aligned} \tag{B.1}$$

According to Bangert *et al* (2013) equation (13), the lateral components $\mathcal{L}_{ij}^{x/y}$ are given by

$$\mathcal{L}_{ij}^{x/y} = \frac{1}{\sqrt{2\pi(\lambda_{ij}^2 + \Sigma_{jj}^{x/y})}} \mathrm{e}^{\frac{\left(x_{ij}/y_{ij} - \mu_j^{x/y}\right)^2}{2\left(\lambda_{ij}^2 + \Sigma_{jj}^{x/y}\right)}} \tag{B.2}$$

where λ_{ij}^2 denotes the variance of the lateral Gaussian beam profile at the respective radiological depth z_{ij}, $\Sigma_{jj}^{x/y}$ denotes the variance of pencil beam j determining the setup error in x/y-dimension, x_{ij}/y_{ij} depicts the lateral distance to the central ray. In analogy, the expected value $\mathcal{Z}_{ij}^\alpha$ of the alpha-dose $\boldsymbol{\alpha}^{\boldsymbol{c}} \circ \boldsymbol{d}$ depth component considering $k = 1...13$ fitted Gaussian components with mean μ_{jk}^α, variance $\delta_{jk}^{\alpha\,2}$ and weight ω_{jk}^α is given by

$$\mathcal{Z}_{ij}^\alpha = \sum_{k=1}^{13} \frac{\omega_{jk}^\alpha}{\sqrt{2\pi(\delta_{jk}^{\alpha\,2} + \Sigma_{jj}^z)}} \mathrm{e}^{\frac{\left(z_{ij} - \mu_{jk}^\alpha\right)^2}{2\left(\delta_{jk}^{\alpha\,2} + \Sigma_{jj}^z\right)}} \tag{B.3}$$

while Σ_{jj}^z denotes the variance of the range error of pencil beam j. Equation (B.3) is in close analogy to equation (16) in Bangert *et al* (2013).

The remaining three components Υ_{ijlm}^x, Υ_{ijlm}^y and $\Xi_{ijlm}^{\sqrt{\beta}}$ represent 2D normal distributions and additionally require the calculation of the co-variance between pencil beams to assess the expectation value of the biological effect. With the 2D vectors $\boldsymbol{x}_{ijlm}$ and $\boldsymbol{\mu}_{jm}^x$ and the 2D matrices Λ_{ijlm}, Σ_{jm}^x

$$\begin{aligned}
\boldsymbol{x}_{ijlm} &= \begin{pmatrix} x_{ij} \\ x_{lm} \end{pmatrix}, \quad \boldsymbol{\mu}_{jm}^x = \begin{pmatrix} \mu_j \\ \mu_m \end{pmatrix} \\
\Lambda_{ijlm} &= \begin{pmatrix} \lambda_{ij}^2 & 0 \\ 0 & \lambda_{lm}^2 \end{pmatrix}, \quad \Sigma_{jm}^x = \begin{pmatrix} \Sigma_{jj}^x & \Sigma_{jm}^x \\ \Sigma_{mj}^x & \Sigma_{mm}^x \end{pmatrix}
\end{aligned} \tag{B.4}$$

the second raw moment of the lateral dose component in the x-dimension Υ_{ijlm}^x is given by

$$\Upsilon_{ijlm}^x = \frac{1}{2\pi\sqrt{|\Lambda_{ijlm} + \Sigma_{jm}^x|}} \mathrm{e}^{-\frac{1}{2}(\boldsymbol{x}_{ijlm} - \boldsymbol{\mu}_{jm}^x)^T (\Lambda_{ijlm} + \Sigma_{jm}^x)^{-1} (\boldsymbol{x}_{ijlm} - \boldsymbol{\mu}_{jm}^x)}. \tag{B.5}$$

Similar deviations can be found in Bangert *et al* (2013) in equation (14). Finally, the second raw moment $\Xi_{ijlm}^{\sqrt{\beta}}$ of the $\sqrt{\boldsymbol{\beta}} \circ \boldsymbol{d}$ component can be calculated by defining:

$$\boldsymbol{z}_{ijlm} = \begin{pmatrix} z_{ij} \\ z_{lm} \end{pmatrix}, \quad \boldsymbol{\mu}_{jumv}^{z} = \begin{pmatrix} \mu_{ju}^{\beta} \\ \mu_{mv}^{\beta} \end{pmatrix}$$
$$\Theta_{jumv}^{\beta} = \begin{pmatrix} {\delta_{ju}^{\beta}}^2 & 0 \\ 0 & {\delta_{mv}^{\beta}}^2 \end{pmatrix}, \quad \Sigma_{jm}^{z} = \begin{pmatrix} \Sigma_{jj}^{z} & \Sigma_{jm}^{z} \\ \Sigma_{mj}^{z} & \Sigma_{mm}^{z} \end{pmatrix}. \tag{B.6}$$

Following the deviation made in equation (18) (Bangert *et al* 2013) and defining u and v be indices of individual Gaussian components, then $\Xi_{ijlm}^{\sqrt{\beta}}$ results in:

$$\Xi_{ijlm}^{\sqrt{\beta}} = \sum_{uv=1}^{13} \frac{\omega_{ju}^{\beta}\omega_{mv}^{\beta}}{2\pi\sqrt{|\Theta_{jumv}^{\beta} + \Sigma_{jm}^{z}|}} \mathrm{e}^{-\frac{1}{2}(\boldsymbol{z}_{ijlm}-\boldsymbol{\mu}_{jumv}^{z})^{T}(\Theta_{jumv}^{\beta}+\Sigma_{jm}^{z})^{-1}(\boldsymbol{z}_{ijlm}-\boldsymbol{\mu}_{jumv}^{z})}. \tag{B.7}$$

Appendix C. Calculation of variance of the biological effect

Let i, l be voxel indices, j, m, o, q be pencil beam indices, and B be the total number of pencil beams, then the full analytical calculation of the covariance of the biological effect requires mixed terms $\mathbb{E}[\varepsilon_i\varepsilon_l]$, which can be calculated as follows:

$$\begin{aligned}
\mathbb{E}[\varepsilon_i\varepsilon_l] &= \int \mathrm{d}\boldsymbol{\Delta}^x \mathrm{d}\boldsymbol{\Delta}^y \mathrm{d}\boldsymbol{\Delta}^z p(\boldsymbol{\Delta}^x)\, p(\boldsymbol{\Delta}^y)\, p(\boldsymbol{\Delta}^z)\, p(\boldsymbol{\Delta}^z) \epsilon_i(\boldsymbol{\Delta}^x, \boldsymbol{\Delta}^y, \boldsymbol{\Delta}^z) \epsilon_l(\boldsymbol{\Delta}^x, \boldsymbol{\Delta}^y, \boldsymbol{\Delta}^z) \\
&= \int \mathrm{d}\boldsymbol{\Delta}^x \mathrm{d}\boldsymbol{\Delta}^y \mathrm{d}\boldsymbol{\Delta}^z p(\boldsymbol{\Delta}^x)\, p(\boldsymbol{\Delta}^y)\, p(\boldsymbol{\Delta}^z)\, p(\boldsymbol{\Delta}^z) \\
&\quad \left\{ \sum_{j}^{B} w_j L_{ij}^x L_{ij}^y Z_{ij}^{\alpha} + \left(\sum_{j}^{B} w_j L_{ij}^x L_{ij}^y Z_{ij}^{\sqrt{\beta}} \right)^2 \right\} \\
&\quad \left\{ \sum_{m}^{B} w_m L_{lm}^x L_{lm}^y Z_{lm}^{\alpha} + \left(\sum_{m}^{B} w_m L_{lm}^x L_{lm}^y Z_{lm}^{\sqrt{\beta}} \right)^2 \right\}
\end{aligned} \tag{C.1}$$

$$\begin{aligned}
&= \sum_{jm}^{B} w_j w_m \left\{ \int \mathrm{d}\boldsymbol{\Delta}^x p(\boldsymbol{\Delta}^x) L_{ij}^x L_{lm}^x \right\} \left\{ \int \mathrm{d}\boldsymbol{\Delta}^y p(\boldsymbol{\Delta}^y) L_{ij}^x L_{lm}^x \right\} \left\{ \int \mathrm{d}\boldsymbol{\Delta}^x p(\boldsymbol{\Delta}^x) Z_{ij}^{\alpha} Z_{lm}^{\alpha} \right\} \\
&\quad + \sum_{jmq}^{B} w_j w_m w_q \left\{ \int \mathrm{d}\boldsymbol{\Delta}^x p(\boldsymbol{\Delta}^x) L_{ij}^x L_{lm}^x L_{lq}^x \right\} \left\{ \int \mathrm{d}\boldsymbol{\Delta}^y p(\boldsymbol{\Delta}^y) L_{ij}^y L_{lm}^y L_{lq}^y \right\} \left\{ \int \mathrm{d}\boldsymbol{\Delta}^z p(\boldsymbol{\Delta}^z) Z_{ij}^{\alpha} Z_{lm}^{\sqrt{\beta}} Z_{lq}^{\sqrt{\beta}} \right\} \\
&\quad + \sum_{jmo}^{B} w_j w_m w_o \left\{ \int \mathrm{d}\boldsymbol{\Delta}^x p(\boldsymbol{\Delta}^x) L_{ij}^x L_{lm}^x L_{io}^x \right\} \left\{ \int \mathrm{d}\boldsymbol{\Delta}^y p(\boldsymbol{\Delta}^y) L_{ij}^y L_{lm}^y L_{io}^y \right\} \left\{ \int \mathrm{d}\boldsymbol{\Delta}^z p(\boldsymbol{\Delta}^z) Z_{ij}^{\alpha} Z_{lm}^{\sqrt{\beta}} Z_{io}^{\sqrt{\beta}} \right\} \\
&\quad + \sum_{jmoq}^{B} w_j w_m w_o w_q \left\{ \int \mathrm{d}\boldsymbol{\Delta}^x p(\boldsymbol{\Delta}^x) L_{ij}^x L_{io}^x L_{lm}^x L_{lq}^x \right\} \left\{ \int \mathrm{d}\boldsymbol{\Delta}^y p(\boldsymbol{\Delta}^y) L_{ij}^y L_{io}^y L_{lm}^y L_{lq}^y \right\} \\
&\quad \left\{ \int \mathrm{d}\boldsymbol{\Delta}^z p(\boldsymbol{\Delta}^z) Z_{ij}^{\sqrt{\beta}} Z_{io}^{\sqrt{\beta}} Z_{lm}^{\sqrt{\beta}} Z_{lq}^{\sqrt{\beta}} \right\}
\end{aligned} \tag{C.2}$$

$$\mathbb{E}[\varepsilon_i\varepsilon_l] = \sum_{jm}^{B} w_j w_m \Upsilon^x_{ijlm}\Upsilon^y_{ijlm}\Xi^{\alpha}_{ijlm} + 2\sum_{jmo}^{B} w_j w_m w_o \Upsilon^x_{ijlmio}\Upsilon^y_{ijlmio}\Xi^{\alpha 2\surd\beta}_{ijlmio} + \sum_{jmoq}^{B} w_j w_m w_o w_q \Upsilon^x_{ijiolmlq}\Upsilon^y_{ijiolmlq}\Xi^{\surd\beta}_{ijiolmlq}. \tag{C.3}$$

Considering only the variance, which is stored in the diagonal of the covariance matrix, we can set $i = l$ and can then obtain:

$$\mathbb{E}[\varepsilon_i\varepsilon_i] = \sum_{jm}^{B} w_j w_m \Upsilon^x_{ijm}\Upsilon^y_{ijm}\Xi^{\alpha}_{ijm} + 2\sum_{jmo}^{B} w_j w_m w_o \Upsilon^x_{ijmo}\Upsilon^y_{ijmo}\Xi^{\alpha 2\surd\beta}_{ijmo} + \sum_{jmoq}^{B} w_j w_m w_o w_q \Upsilon^x_{ijmoq}\Upsilon^y_{ijmoq}\Xi^{\surd\beta}_{ijmoq}. \tag{C.4}$$

As an example, the calculation of $\Xi^{\alpha 2\surd\beta}_{ijlmpq}$ is shown below (calculations for $\Upsilon^{x/y}_{ijlmpq}$ can be done in a similar fashion). Given that i, l, p depict voxel indices, j, m, q spot indices and u,v,w individual Gaussian components, we can define

$$\boldsymbol{z}_{ijlmpq} = \begin{pmatrix} z_{ij} \\ z_{lm} \\ z_{pq} \end{pmatrix}, \quad \boldsymbol{\mu}^z_{jumvqw} = \begin{pmatrix} \mu^{\alpha}_{ju} \\ \mu^{\beta}_{mv} \\ \mu^{\beta}_{qw} \end{pmatrix} \quad \boldsymbol{\Delta}^z_{jmq} = \begin{pmatrix} \Delta^z_j \\ \Delta^z_m \\ \Delta^z_q \end{pmatrix}$$
$$\Theta_{jumvqw} = \begin{pmatrix} {\delta^{\alpha}_{ju}}^2 & 0 & 0 \\ 0 & {\delta^{\beta}_{mv}}^2 & 0 \\ 0 & 0 & {\delta^{\beta}_{qw}}^2 \end{pmatrix}, \quad \Sigma^z_{jmq} = \begin{pmatrix} \Sigma^z_{jj} & \Sigma^z_{mj} & \Sigma^z_{qj} \\ \Sigma^z_{jm} & \Sigma^z_{mm} & \Sigma^z_{qm} \\ \Sigma^z_{jq} & \Sigma^z_{mq} & \Sigma^z_{qq} \end{pmatrix} \tag{C.5}$$

to solve

$$\begin{aligned}
\Xi^{\alpha 2\surd\beta}_{ijlmpq} &= \int \mathrm{d}\boldsymbol{\Delta}^z p(\boldsymbol{\Delta}^z) Z^{\alpha}_{ij} Z^{\surd\beta}_{lm} Z^{\surd\beta}_{pq} \\
&= \int \mathrm{d}\boldsymbol{\Delta}^z p(\boldsymbol{\Delta}^z) \sum_{uvw=1}^{13} \frac{\omega^{\alpha}_{ju}}{\sqrt{2\pi{\delta^{\alpha}_{ju}}^2}} \mathrm{e}^{\frac{(z_{ij}-\mu^{\alpha}_{ju})^2}{2{\delta^{\alpha}_{ju}}^2}} \frac{\omega^{\beta}_{mv}}{\sqrt{2\pi{\delta^{\beta}_{mv}}^2}} \mathrm{e}^{\frac{(z_{lm}-\mu^{\beta}_{mv})^2}{2{\delta^{\beta}_{mv}}^2}} \frac{\omega^{\beta}_{qw}}{\sqrt{2\pi{\delta^{\beta}_{qw}}^2}} \mathrm{e}^{\frac{(z_{pq}-\mu^{\beta}_{qw})^2}{2{\delta^{\beta}_{qw}}^2}} \\
&= \int \mathrm{d}\boldsymbol{\Delta}^z p(\boldsymbol{\Delta}^z) \sum_{uvw=1}^{13} \frac{\omega^{\alpha}_{ju}\omega^{\beta}_{mv}\omega^{\beta}_{qw}}{(2\pi)^{\frac{3}{2}}\sqrt{|\Theta_{jumvqw}|}} \mathrm{e}^{-\frac{1}{2}(\boldsymbol{z}_{ijlmpq}-\boldsymbol{\mu}^z_{jumvqw})^T(\Theta_{jumvqw})^{-1}(\boldsymbol{z}_{ijlmpq}-\boldsymbol{\mu}^z_{jumvqw})} \\
&= \sum_{uvw=1}^{13} \omega^{\alpha}_{ju}\omega^{\beta}_{mv}\omega^{\beta}_{qw} \int \mathrm{d}\boldsymbol{\Delta}^z_{jmq} \frac{1}{(2\pi)^{\frac{3}{2}}\sqrt{|\Sigma^z_{jmq}|}} \\
&\quad \frac{1}{(2\pi)^{\frac{3}{2}}\sqrt{|\Theta_{jumvqw}|}} \mathrm{e}^{-\frac{1}{2}(\boldsymbol{z}_{ijlmpq}-\boldsymbol{\mu}^z_{jumvqw})^T(\Theta_{jumvqw})^{-1}(\boldsymbol{z}_{ijlmpq}-\boldsymbol{\mu}^z_{jumvqw})} \\
&= \sum_{uvw=1}^{13} \frac{\omega^{\alpha}_{ju}\omega^{\beta}_{mv}\omega^{\beta}_{qw}}{(2\pi)^{\frac{3}{2}}\sqrt{|\Theta_{jumvqw}+\Sigma^z_{jmq}|}} \mathrm{e}^{-\frac{1}{2}(\boldsymbol{z}_{ijlmpq}-\boldsymbol{\mu}^z_{jumvqw})^T(\Theta_{jumvqw}+\Sigma^z_{jmq})^{-1}(\boldsymbol{z}_{ijlmpq}-\boldsymbol{\mu}^z_{jumvqw})}.
\end{aligned} \tag{C.6}$$

Calculations for $\Upsilon^{x/y}_{ijlmpqno}$ and $\Xi^{\sqrt{\beta}}_{ijlmpqno}$ are not explicitly stated here as their deviations are in close analogy to $\Xi^{\alpha 2\sqrt{\beta}}_{ijlmpq}$. Instead of integrating over a 3D Gaussian, the integration is thereby conducted over 4D Gaussian distributions.

ORCID iDs

H P Wieser https://orcid.org/0000-0002-2309-7963
N Wahl https://orcid.org/0000-0002-1451-223X

References

Albertini F, Hug E B and Lomax A J 2011 Is it necessary to plan with safety margins for actively scanned proton therapy? *Phys. Med. Biol.* **56** 4399–413
Anderson T V and Mattson C A 2012 Propagating skewness and kurtosis through engineering models for low-cost, meaningful, nondeterministic design *J. Mech. Des.* **134** 100911
Bangert M, Hennig P and Oelfke U 2013 Analytical probabilistic modeling for radiation therapy treatment planning *Phys. Med. Biol.* **58** 5401–19
Baum C, Alber M, Birkner M and Nüsslin F 2004a Treatment simulation approaches for the estimation of the distributions of treatment quality parameters generated by geometrical uncertainties *Phys. Med. Biol.* **49** 5475–88
Chen W, Unkelbach J, Trofimov A, Madden T, Kooy H, Bortfeld T and Craft D 2012 Including robustness in multi-criteria optimization for intensity-modulated proton therapy *Phys. Med. Biol.* **57** 591–608
Elsässer T *et al* 2010 Quantification of the relative biological effectiveness for ion beam radiotherapy: direct experimental comparison of proton and carbon ion beams and a novel approach for treatment planning *Int. J. Radiat. Oncol. Biol. Phys.* **78** 1177–83
Fredriksson A, Forsgren A and Hardemark B 2011 Minimax optimization for handling range and setup uncertainties in proton therapy *Med. Phys.* **38** 1672–84
Jäkel O, Krämer M, Karger C P and Debus J 2001 Treatment planning for heavy ion radiotherapy: clinical implementation and application *Phys. Med. Biol.* **46** 1101–16
Kamp F, Brüningk S, Cabal G, Mairani A, Parodi K and Wilkens J J 2014 Variance-based sensitivity analysis of biological uncertainties in carbon ion therapy *Phys. Med.* **30** 583–7
Kellerer A M and Rossi H H 1978 A generalized formulation of dual radiation action *Radiat. Res.* **75** 471
Krämer M and Scholz M 2006 Rapid calculation of biological effects in ion radiotherapy *Phys. Med. Biol.* **51** 1959–70
Liu W, Frank S J, Li X, Li Y, Park P C, Dong L, Ronald Zhu X and Mohan R 2013 Effectiveness of robust optimization in intensity-modulated proton therapy planning for head and neck cancers *Med. Phys.* **40** 051711
Liu W, Zhang X, Li Y and Mohan R 2012 Robust optimization of intensity modulated proton therapy *Med. Phys.* **39** 1079–91
Lomax A J 2008a Intensity modulated proton therapy and its sensitivity to treatment uncertainties 1: the potential effects of calculational uncertainties *Phys. Med. Biol.* **53** 1027–42
Lomax A J 2008b Intensity modulated proton therapy and its sensitivity to treatment uncertainties 2: the potential effects of inter-fraction and inter-field motions *Phys. Med. Biol.* **53** 1043–56
Lomax A J 2008c Intensity modulated proton therapy *Proton and Charged Particle Radiotherapy* ed T Delaney and H Kooy (Philadelphia, PA: Lippincott Williams and Wilkins)
Low D A, Harms W B, Mutic S and Purdy J A 1998 A technique for the quantitative evaluation of dose distributions *Med. Phys.* **25** 656
Lowe M, Albertini F, Aitkenhead A, Lomax A J and MacKay R I 2016 Incorporating the effect of fractionation in the evaluation of proton plan robustness to setup errors *Phys. Med. Biol.* **61** 413–29
Paganetti H 2012 Range uncertainties in proton therapy and the role of Monte Carlo simulations *Phys. Med. Biol.* **57** R99–R117
Park P C, Cheung J, Zhu X R, Sahoo N, Court L and Dong L 2012 Fast range-corrected proton dose approximation method using prior dose distribution *Phys. Med. Biol.* **57** 3555–69

Perkó Z, van der Voort S R, van de Water S, Hartman C M H, Hoogeman M and Lathouwers D 2016 Fast and accurate sensitivity analysis of IMPT treatment plans using polynomial chaos expansion *Phys. Med. Biol.* **61** 4646–64

Pflugfelder D, Wilkens J J and Oelfke U 2008 Worst case optimization: a method to account for uncertainties in the optimization of intensity modulated proton therapy *Phys. Med. Biol.* **53** 1689–700

Sakama M, Kanematsu N and Inaniwa T 2016 A robustness analysis method with fast estimation of dose uncertainty distributions for carbon–ion therapy treatment planning *Phys. Med. Biol.* **61** 5818–36

Schaffner B, Pedroni E and Lomax A 1999 Dose calculation models for proton treatment planning using a dynamic beam delivery system: an attempt to include density heterogeneity effects in the analytical dose calculation *Phys. Med. Biol.* **44** 27–41

Scholz M and Kraft G 1996 Track structure and the calculation of biological effects of heavy charged particles *Adv. Space Res.* **18** 5–14

Siggel M, Ziegenhein P, Nill S and Oelfke U 2012 Boosting runtime-performance of photon pencil beam algorithms for radiotherapy treatment planning *Phys. Med.* **28** 273–80

Sobotta B, Söhn M and Alber M 2012 Accelerated evaluation of the robustness of treatment plans against geometric uncertainties by Gaussian processes *Phys. Med. Biol.* **57** 8023–39

Squires G L 2001 *Practical Physics* (Cambridge: Cambridge University Press) (https://doi.org/10.1017/CBO9781139164498)

Steitz J, Naumann P, Ulrich S, Haefner M F, Sterzing F, Oelfke U and Bangert M 2016 Worst case optimization for interfractional motion mitigation in carbon ion therapy of pancreatic cancer *Radiat. Oncol.* **11** 134

Suit H *et al* 2010 Proton versus carbon ion beams in the definitive radiation treatment of cancer patients *Radiother. Oncol.* **95** 3–22

Unkelbach J, Bortfeld T, Martin B C and Soukup M 2009 Reducing the sensitivity of IMPT treatment plans to setup errors and range uncertainties via probabilistic treatment planning *Med. Phys.* **36** 149–63

Unkelbach J, Chan T C Y and Bortfeld T 2007 Accounting for range uncertainties in the optimization of intensity modulated proton therapy *Phys. Med. Biol.* **52** 2755–73

Unkelbach J and Oelfke U 2004 Inclusion of organ movements in IMRT treatment planning via inverse planning based on probability distributions *Phys. Med. Biol.* **49** 4005–29

Van Herk M 2004 Errors and margins in radiotherapy *Semin. Radiat. Oncol.* **14** 52–64

Wahl N, Hennig P, Wieser H P and Bangert M 2017 Efficency of analytical and sampling-based uncertainty propagation in intensity-modulated proton therapy *Phys. Med. Biol.* **62** 5790–807

Wieser H-P *et al* 2017 Development of the open-source dose calculation and optimization toolkit matRad *Med. Phys.* **44** 2556–68

Wilkens J J and Oelfke U 2006 Fast multifield optimization of the biological effect in ion therapy *Phys. Med. Biol.* **51** 3127–40

Wolf I, Vetter M, Wegner I, Böttger T, Nolden M, Schöbinger M, Hastenteufel M, Kunert T and Meinzer H-P 2005 The medical imaging interaction toolkit *Med. Image Anal.* **9** 594–604

Zaider M and Rossi H H 1980 The synergistic effects of different radiations *Radiat. Res.* **83** 732–9